NIST Special Publication 260
NIST SP 260-241

Development of Reference Material 8103

Adamantane for Subambient DSC Temperature and Enthalpy Calibration

Tara J. Fortin
Amanda A. Koepke
Jolene D. Splett

This publication is available free of charge from:
https://doi.org/10.6028/NIST.SP.260-241

NIST NATIONAL INSTITUTE OF STANDARDS AND TECHNOLOGY
U.S. DEPARTMENT OF COMMERCE

NIST Special Publication 260
NIST SP 260-241

Development of Reference Material 8103

Adamantane for Subambient DSC Temperature and Enthalpy Calibration

Tara J. Fortin
Applied Chemicals and Materials Division
Material Measurement Laboratory

Amanda A. Koepke
Jolene D. Splett*
Statistical Engineering Division
Information Technology Laboratory

**Former NIST employee; all work for this publication was done while at NIST.*

This publication is available free of charge from:
https://doi.org/10.6028/NIST.SP.260-241

September 2024

U.S. Department of Commerce
Gina M. Raimondo, Secretary

National Institute of Standards and Technology
Laurie E. Locascio, NIST Director and Under Secretary of Commerce for Standards and Technology

NIST SP 260-241
September 2024

Certain equipment, instruments, software, or materials, commercial or non-commercial, are identified in this paper in order to specify the experimental procedure adequately. Such identification does not imply recommendation or endorsement of any product or service by NIST, nor does it imply that the materials or equipment identified are necessarily the best available for the purpose.

NIST Technical Series Policies
Copyright, Use, and Licensing Statements
NIST Technical Series Publication Identifier Syntax

Publication History
Approved by the NIST Editorial Review Board on 2023-10-19

How to Cite this NIST Technical Series Publication
Fortin TJ, Koepke AA, Splett JD (2024) Development of Reference Material 8103: Adamantane for Subambient DSC Temperature and Enthalpy Calibration. (National Institute of Standards and Technology, Gaithersburg, MD), NIST Special Publication 260 (SP) NIST SP 260-241. https://doi.org/10.6028/NIST.SP.260-241

Author ORCID iDs
Tara J. Fortin: 0000-0001-6150-8930
Amanda A. Koepke: 0000-0001-9515-0383

Abstract

A new Reference Material (RM), designated RM 8013, has been developed for the temperature and enthalpy calibration of differential scanning calorimeters (DSCs). The addition of this new RM expands the applicable range of NIST's DSC-related calibration standards to include sub-ambient temperatures and represents an attractive alternative to the previous option, Standard Reference Material® (SRM®) 2225 Mercury, which was discontinued in 2017. RM 8103 was sourced from a single lot of high-purity (≥ 99%) adamantane. The transition temperature of RM 8103 has been determined to be equal to (-64.58 ± 0.20) °C, while the enthalpy of transition has been determined to be equal to (21.64 ± 0.34) $J \cdot g^{-1}$. Both values were determined via DSC measurements using an instrument calibrated with certified reference materials obtained from two different national metrology institutes. This document provides all relevant measurement and analysis details for the development of RM 8103.

Keywords

Adamantane, Calibration, Differential scanning calorimetry, Differential thermal analyzers, Enthalpy of transition, Transition temperature.

Table of Contents

List of Tables

List of Figures

Acknowledgments

The authors thank our NIST colleagues Dr. Megan Harries and Dr. Jason Widegren for providing the compositional analysis and water content analysis of the adamantane RM sample lot.

1. Introduction

Differential Scanning Calorimeters (DSCs) are regularly used in numerous applications including, but not limited to, materials characterization, the evaluation of phase diagrams, purity determinations, kinetic investigations, and heat capacity measurements. DSCs have largely replaced classical precision calorimeters, such as adiabatic calorimeters, because they require smaller sample volumes, less time, and less specialized expertise to run. However, since DSC is not an absolute measurement technique, calibration is essential to ensure the accuracy of measured temperature, enthalpy, and heat capacity. Over the years, NIST has offered several certified Standard Reference Materials® (SRMs®) to support high-quality calibrations for DSC (e.g., SRM 720 Sapphire, SRM 2220 Tin, SRM 2221a Zinc, SRM 2232 Indium, SRM 2234 Gallium, and SRM 2235 Bismuth). One such standard, SRM 2225 Mercury, represented the only available certified reference material for the low-temperature calibration of DSCs. However, safety concerns ultimately led to its discontinuation in late 2017.

Adamantane has been identified as a potential low-temperature calibration material [1, 2]. It undergoes a crystalline rearrangement, from a face-centered cubic to a body-centered tetragonal lattice, at approximately -64 °C [3, 4]. This, combined with its low toxicity, low vapor pressure, and low reactivity, make adamantane an ideal candidate as a calibrant and an attractive alternative to mercury. Therefore, NIST has developed an adamantane reference material for the low-temperature calibration of DSCs. The new reference material is designated RM 8103 and the solid-solid transition temperature (t_{tran}) and enthalpy of transition (ΔH_{tran}) values are shown in Table 1, along with the associated expanded uncertainties.

Table 1. RM 8103 Transition Temperature (t_{tran}) and Enthalpy of Transition (ΔH_{tran}) Values[a] with Expanded[b] Uncertainties.

t_{tran}	=	(-64.58 ± 0.20) °C
ΔH_{tran}	=	(21.64 ± 0.34) J·g^{-1}

[a]At thermal equilibrium (i.e., zero heating rate).
[b]Uncertainty interval with 95% confidence level (*k* = 1.96 and *k* = 1.92, respectively).

A unit of RM 8103 consists of approximately 1 g of material sealed in a 10 mL amber glass bottle; the material was sourced from a single lot of high-purity (≥ 99%) adamantane. The development of RM 8103 largely followed the same general procedures as were utilized during the certification of NIST's most popular DSC calibration standard, SRM 2232 [5], but with a few key differences, including improvements implemented to comply with evolving requirements. Here, the determination of both the transition temperature and the enthalpy of transition employed DSC measurements on 15 samples randomly selected from the RM lot. The DSC used for these measurements was calibrated using certified reference materials from two different

national metrology institutes: NIST and Physikalisch-Technische Bundesanstalt (PTB).[1] Details of the materials and measurement methods employed, as well as the associated uncertainty analysis, are provided in the subsequent text.

[1] Certain equipment, instruments, software, or materials, commercial or non-commercial, are identified in this paper in order to specify the experimental procedure adequately. Such identification does not imply recommendation or endorsement of any product or service by NIST, nor does it imply that the materials or equipment identified are necessarily the best available for the purpose.

2. Materials and Methods

2.1. High-Purity Adamantane

A total of 700 g of material from a single lot of high purity (≥ 99%) adamantane (lot # MKCL1826) was purchased from Sigma-Aldrich Inc., St. Louis, MO. As purchased, the material was packaged in seven sealed plastic bottles, each containing 100 g of adamantane. Approximately 500 g of this material was subsequently re-packaged as ~ 1 g aliquots sealed in 10 mL amber glass bottles by the NIST Office of Reference Materials for distribution as RM 8103.

In an effort to independently verify sample purity, as well as to check lot homogeneity, six samples of adamantane were submitted to NIST colleagues in the Fluid Characterization Group of the Applied Chemicals and Materials Division for analysis. Specifically, samples from six of the seven adamantane bottles (labeled "A" – "F") were transferred to clean 20 mL glass bottles (also labeled "A" – "F"). Care was taken to thoroughly mix the contents of each source bottle prior to and during sampling. The contents from these six 20 mL bottles were used to prepare DSC measurement samples (see Sec. 2.2.2) prior to submitting the remaining contents for purity and water content analysis.

Sample purity was assessed using gas chromatography-mass spectrometry (GC-MS). The GC-MS analysis did not detect any impurities above the instrument's detection limit for any of the six adamantane samples, resulting in an estimated purity of (100 ± 0.1) % (see Fig. A.1.1 of Appendix A1). Water content was determined via Karl Fischer (KF) titration and ranged from a minimum of (383.5 ± 81.5) $\mu g \cdot g^{-1}$ for sample A to a maximum of (453.1 ± 45.6) $\mu g \cdot g^{-1}$ for sample D (see Fig. A.1.2 of Appendix A1). Thus, within the estimated combined expanded uncertainties, the water content was the same for all six RM samples. The lack of statistically significant differences between the six RM samples in either the GC-MS or KF titration results indicates lot homogeneity.

2.2. Determination of Transition Temperature and Enthalpy of Transition

2.2.1. Instrument Calibration

A Q2000 DSC from TA Instruments was utilized for the determination of both the transition temperature and the enthalpy of transition for RM 8103. Prior to measurements of the RM lot material, careful calibration of the instrument was required to ensure the accuracy of measured temperature and enthalpy. First, an instrument-specific calibration, referred to as a Tzero™ calibration, was performed to adjust the instrument's baseline and correct for cell asymmetries. Next, temperature and enthalpy were calibrated via measurements of pure materials with well-known melting temperatures (t_m) and enthalpies of fusion (ΔH_{fus}). In this work, two certified reference materials were used for calibration measurements: indium from PTB (SN KM-31402, t_m = 156.598 ± 0.004 °C, ΔH_{fus} = 28.64 ± 0.06 $J \cdot g^{-1}$) [6] and mercury from NIST (SRM 2225, t_m = -38.85 ± 0.03 °C, ΔH_{fus} = 11.469 ± 0.008 $J \cdot g^{-1}$) [7]. Certified values for both reference materials

include expanded (k = 2) uncertainties. The indium reference material was certified via comparison with a fixed-point standard and measurements using a modified Tian-Calvet calorimeter for temperature and enthalpy, respectively [6]. The mercury reference material was certified via adiabatic calorimetry for both temperature and enthalpy [7]. It should be noted that the certified fusion temperature for mercury was converted to the ITS-90 temperature scale [8] for use in this work.

The determination of both the temperature and enthalpy calibration parameters are represented schematically in Fig. 1, where the gray line represents a theoretical melting curve. The temperature used is the extrapolated onset temperature (t_e), which is determined from the intersection of the inflectional tangent line (red dashed line) and the interpolated baseline (blue dashed line) (Fig. 1). This is used instead of the peak maximum/minimum temperature because it is less dependent on the heating rate and sample parameters such as sample thermal conductivity, sample mass, and sample thickness [9-11].

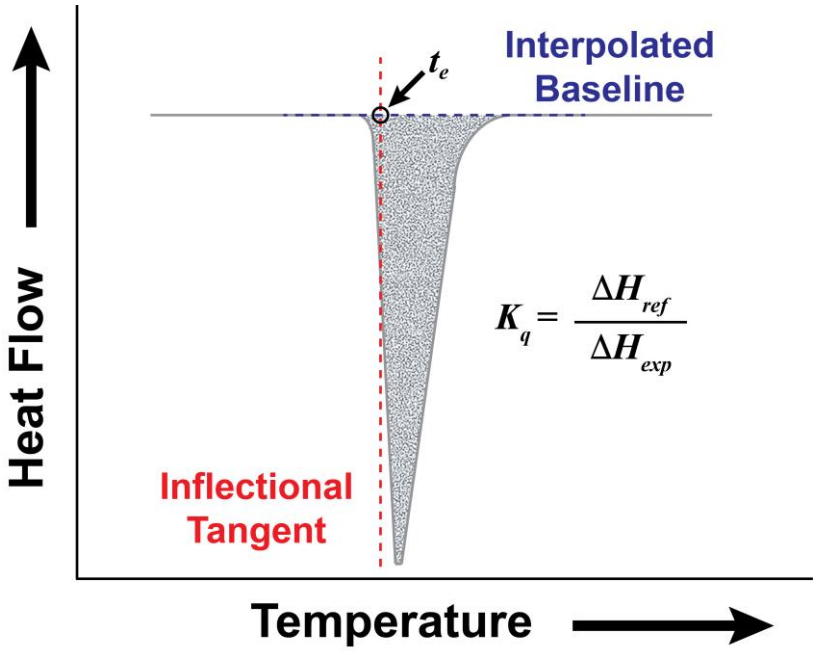

Figure 1. Determination of temperature and enthalpy calibration parameters. The gray line represents a theoretical melting curve. The extrapolated onset temperature (t_e) is used for the temperature calibration. The integrated peak area (shaded gray) is used to determine the enthalpy calibration coefficient (K_q).

With DSC, energy is determined by integrating the heat flow signal over time and multiplying by a proportionality constant (K_q). K_q is calculated by dividing the reference transition enthalpy (ΔH_{ref}) by the experimental transition enthalpy (ΔH_{exp}) (see Fig. 1). The certified values obtained from the respective calibration certificates were used for the former, while the latter was obtained by integrating the experimentally determined melting curves (shaded gray in Fig. 1).

In this work, five samples for each of the two calibration materials were encapsulated in hermetically sealed aluminum pans. All mass measurements employed a microbalance and a double-substitution (ABBA) weighing scheme [12]; additional details regarding sample preparation can be found in Fortin et al. [13]. For the certified indium samples, masses ranged from 7.021 mg to 12.660 mg, including two samples with masses of ~ 8.0 mg. The certified mercury sample masses ranged from 6.750 mg to 13.265 mg and included two samples with masses of ~ 8.6 mg. It should be noted that aluminum can form an amalgam in solution with mercury. However, in this work, no evidence of this was observed in either the experimental data or upon inspection of the sample pans after measurements were completed.

For all calibration measurements the procedure was as follows. A sample pan was loaded into the measurement cell, along with an empty reference pan (also hermetically sealed and aluminum). The cell was then equilibrated at a temperature significantly below the melting point (i.e., 100 °C and -80 °C for indium and mercury, respectively) before heating at a given heating rate (β) to a temperature sufficiently above the melting point to reestablish a stable baseline (i.e., 180 °C and 0 °C for indium and mercury, respectively). Since the primary measurements associated with DSC are very sensitive to the specific experimental conditions employed (e.g., the sample size and form, sample placement within the pan, pan type, pan placement within the cell, heating rate employed, purge gas used, etc.), temperature and enthalpy calibrations should be carried out using the same conditions as will be used for sample measurements [9-11]. Therefore, after an initial "premelt" run at β = 20 °C·min^{-1}, each sample pan was measured twice at each of four heating rates in the order: 1 °C·min^{-1}, 10 °C·min^{-1}, 3 °C·min^{-1}, and 5 °C·min^{-1}. Sample pan selection was randomized but no back-to-back runs of a given pan were permitted; this was done to ensure that a sample pan was always placed anew at the start of each run thus capturing any variability in the results attributable to pan placement. All indium calibration measurements at a given heating rate were completed before moving on to the next heating rate, and all indium measurements were completed before repeating the procedure with the certified mercury samples. Additionally, at each heating rate, multiple baseline checks were performed before, during, and after calibration measurements to check for evidence of deterioration in the instrument's performance; no such evidence was observed. Finally, for all measurements, dry nitrogen was used as a purge gas at a flow rate of 50 mL·min^{-1}.

Upon completion of the calibration measurements, the individual melting curves were analyzed to determine both t_e and K_q. Although several literature sources recommend extrapolating to zero heating rate to determine a temperature correction [14, 15], the ASTM standard test method for DSC temperature calibration (E967) [16] calls for calibration at the heating rate of interest. We have used the β-specific approach in this work. Therefore, an overall average t_e, encompassing all sample sizes and replicate measurements, was calculated for each heating rate for both indium and mercury; the results are reported in Table 2. Prior to the start of RM 8103 adamantane measurements at a given heating rate, the corresponding calibration parameters were entered into the instrument's software. It should be noted that for a two-point calibration the instrument's software uses the entered temperatures to calculate a slope and intercept which are then used to interpolate between the two endpoints; when extrapolating to temperatures either below or above the entered endpoints, the instrument's

software assumes a slope of one and applies the corresponding offset. For the enthalpy calibration, we followed literature recommendations [14, 15] and determined K_q as a function of temperature, as well as heating rate. However, since no significant mass dependence was observed in the calibration data and indium's enthalpy of fusion is similar to adamantane's enthalpy of transition, we ultimately used the indium results alone to calculate an average K_q including all sample masses and replicate measurements. The resulting β-specific values, which are reported in Table 2, were used for all subsequent RM 8103 adamantane measurements.

Table 2. Instrument Calibration Parameters Used During RM 8103 Measurements.

β^a (°C·min^{-1})	Mercury $t_e{}^b$ (°C)	Indium $t_e{}^b$ (°C)	$K_q{}^c$
1	-37.845	156.398	1.05260
3	-37.875	156.427	1.05365
5	-37.907	156.438	1.05485
10	-37.973	156.390	1.05416

[a]Nominal heating rate. [b]Averaged extrapolated onset temperature. [c]Averaged enthalpy calibration coefficient.

2.2.2. RM Adamantane Temperature and Enthalpy Measurements

For the RM 8103 measurements, a total of 15 samples were prepared from the RM sample lot. Specifically, samples from six of the seven adamantane bottles (labeled "A" – "F") were transferred to clean 20 mL glass bottles (also labeled "A" – "F"), the contents of which were then used to prepare the DSC measurement samples. To randomize sample selection, the contents of each 100 g source bottle, as well as the six 20 mL bottles, were thoroughly mixed prior to and during sampling. For each sample bottle, a freshly cleaned spatula was used for the mixing and transfer of sample. All DSC measurement samples were encapsulated in hermetically sealed aluminum pans and the sample was lightly packed using a specialized powdered sample tool prior to sealing. Additional information regarding sample preparation can be found in Sec. 2.2.1 and the references cited therein. Overall, RM adamantane sample masses ranged from 7.314 mg to 14.502 mg, with several samples of ~ 8.4 mg. Individual sample masses are reported in Table 3.

In addition to the RM adamantane samples listed in Table 3, additional samples were prepared to check the calibrated instrument's performance against certified temperature and enthalpy values. Specifically, three fresh samples of the mercury calibration material were prepared with masses of 6.677 mg, 8.953 mg, and 12.337 mg.

The RM 8103 transition temperature and enthalpy of transition measurements followed the previously described procedure employed for the calibration measurements (see Sec. 2.2.1). The mercury check samples were incorporated with the RM samples during these measurements. As with the calibration samples, all of the RM and check samples underwent an initial "premelt" run at β = 20 °C·min^{-1}. However, for these measurements, each sample was

measured a total of three times at each of the four heating rates (1 °C·min^{-1}, 10 °C·min^{-1}, 3 °C·min^{-1}, and 5 °C·min^{-1}). Prior to measurements at a given heating rate, the corresponding β-specific calibration parameters from Table 2 were entered into the instrument's software. Once again, regular baseline checks were performed during each measurement series. In addition, a single indium verification measurement was performed after each baseline check using one of the ~ 8 mg certified indium samples previously used for the calibration measurements. These baseline and indium verification measurements were used to verify that the instrument was operating within specifications for the duration of the RM 8103 temperature and enthalpy measurements.

Table 3. Adamantane Samples Used for RM 8103 Temperature and Enthalpy Measurements.

Sample	Mass (mg)
A1	8.380
A2	8.402
A3	8.374
A4	8.424
B	7.314
B2	8.415
C1	8.388
C2	8.434
C3	8.402
D	14.459
D2	14.502
E	9.377
E2	9.227
F1	10.825
F2	9.171

3. Experimental Results

3.1. Transition Temperature Results

Upon completion of the RM 8103 adamantane measurements, each of the resulting heat flow curves were analyzed to determine the measured transition temperature (t_{meas}). An example of this analysis is shown in Fig. 2 for sample A4 measured at β = 1 °C·min^{-1}. First, a sigmoidal tangent baseline is drawn between two endpoint pairs on either side of the transition peak; in this example the endpoint pairs are at -75 °C and -74 °C and -54 °C and -53 °C and an expanded view of the baseline is shown in the inset. A sigmoidal tangent baseline is used here instead of a linear baseline because the different heat capacities of the two crystalline phases result in a significant offset between the baselines on either side of the transition peak. Additional details regarding the baseline can be found in Appendix A.2. Next, an inflectional tangent line is constructed at the leading edge of the transition peak; the intersection of this line with the baseline gives the extrapolated onset temperature, t_e, which is used to define the transition temperature.

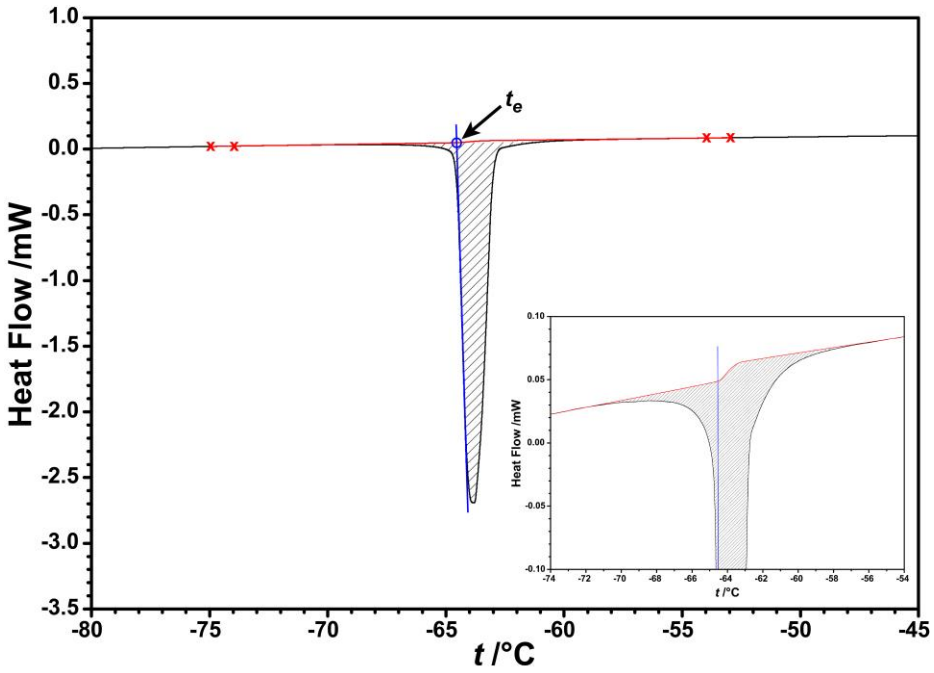

Figure 2. Determination of transition temperature and enthalpy of transition. Shown in black is the heat flow curve plotted as a function of temperature for a single replicate measurement of sample A4 at 1 °C·min^{-1}. A baseline (red) is drawn between points on either side of the peak; a sigmoidal tangent baseline is used for adamantane. An expanded view of the baseline is shown in the inset. In this example, the endpoint pairs are at -75 °C and -74 °C and -54 °C and -53 °C (red x's). The peak is then integrated to get the area (hatch marks) in mW·s, which is divided by the sample mass to obtain the enthalpy of transition. The extrapolated onset temperature (t_e) is used to designate the transition temperature. It is determined by constructing an inflectional tangent line (blue) and finding its point of intersection with the baseline (blue circle).

The results for each individual replicate measurement are reported in Table A.3.1 of Appendix A.3. To aid in comparisons, the t_{meas} results reported in Table A.3.1 are also shown in Fig. 3, plotted as a function of nominal heating rate. Here, the sample source bottles are distinguished by six distinct markers and the bottle subsamples are differentiated by color. The greatest overall variability is observed at β = 10 °C·min^{-1}, while the observed variabilities are similar for the other three heating rates.

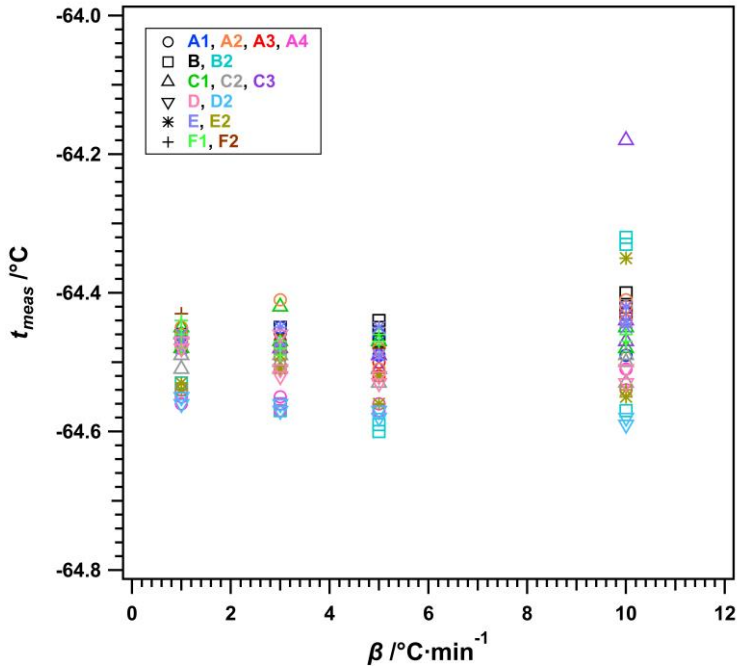

Figure 3. Replicate transition temperature measurement results for fifteen RM 8103 samples plotted as a function of nominal heating rate. Samples sourced from six different 100 g bottles are plotted as distinct markers and bottle-specific subsamples are differentiated by color, as indicated by the included legend.

The goal is to use the measurement results shown in Fig. 3 to derive a single transition temperature and its associated uncertainty for each of the measured heating rates (t_β and $u(t_\beta)$, respectively). However, as was previously discussed, DSC measurements are highly sensitive to experimental parameters such as heating rate, and each individual instrument will presumably exhibit its own particular dependency. As such, β-dependent information is only of limited use; for a reference material the transition temperature at thermal equilibrium is the value of interest for consumers. Therefore, ultimately, we want to determine the transition temperature at β = 0 °C·min^{-1}.

In this work, we have used a hierarchical Bayesian model [17] to determine t_β and $u(t_\beta)$ as a function of heating rate, including at β = 0 °C·min^{-1}. With this type of model, we can easily account for correlations in the data induced by using the same subsamples across different β values. Additionally, this approach is able to handle the fact that the actual β values differ

slightly from the nominal. Specifically, for each measured transition temperature value, we assume

$$t_{meas,ijk} = \alpha_0 + \alpha_1 \cdot \beta_{ijk} + A_i + B_{ij} + \epsilon_{ijk} + S_l \ . \quad (1)$$

Here, α_0 is the intercept, which corresponds to the value at β = 0 °C·min^{-1} (i.e., t_{tran}), and α_1 is the slope. The "ijk" subscript indicates the k^{th} measurement for the j^{th} subsample within the i^{th} sample. In this work, i = 1,...,6 and j = 1,...,$n_{j(i)}$, with the number of subsamples, $n_{j(i)}$, within each sample varying from 1 to 4. A_i accounts for sample effects and is assumed to have a normal distribution with an expected value of zero and a variance of σ_A^2 (i.e., A_i ~ Normal(0, σ_A)). Similarly, B_{ij} accounts for subsample effects and B_{ij} ~ Normal(0, σ_B). Next, ϵ_{ijk} represents the measurement error due to random effects. To allow for possible outlying points, such as subsample 3 of sample C (e.g., sample C3 in Table 3) at β = 10 °C·min^{-1} (see Fig. 3), we assume ϵ_{ijk} has a Student's t-distribution with four degrees of freedom, an expected value of 0, and a scale selected such that its variance is equal to σ_ϵ^2. Finally, S_l represents the β-specific subsample effect with S_l ~ Normal(0, $\sigma_{S,l}$). Here, l indicates the associated nominal heating rate (i.e., $l \in$ 1,...,4 corresponding to β = 1, 3, 5, or 10 °C·min^{-1}). To determine $\sigma_{S,l}$ we calculate the uncertainty due to systematic effects, $u(t_{meas})$, and use the mean at each nominal β. The determination of $u(t_{meas})$ is discussed in detail in Sec. 4.1.

We use a Bayesian analysis to fit the model in Eq. (1). In a Bayesian analysis, we are interested in the posterior distribution of the parameters of interest, $\boldsymbol{\theta} = (\alpha_0, \alpha_1, \sigma_A, \sigma_B, \sigma_\epsilon, \mathbf{A}, \mathbf{B}, \mathbf{S})$, which is proportional to the prior distribution, $p(\boldsymbol{\theta})$, multiplied by the likelihood of the observed data, $p(\mathbf{x}|\boldsymbol{\theta})$. Mathematically, this is written as

$$p(\boldsymbol{\theta}|\mathbf{x}) \propto p(\boldsymbol{\theta})p(\mathbf{x}|\boldsymbol{\theta}). \quad (2)$$

The likelihood, $p(\mathbf{x}|\boldsymbol{\theta})$, is the probability density for the observed data $\mathbf{x} = (\mathbf{t}, \boldsymbol{\beta}, \boldsymbol{\sigma_S})$ given a set of parameters $\boldsymbol{\theta}$. It is determined by the model and distributions described below. Here, $\mathbf{t}$ and $\boldsymbol{\beta}$ represent the $t_{meas,ijk}$ and β_{ijk} for all i, j, and k values and $\boldsymbol{\sigma_S}$ represents $\sigma_{S,l}$ for $l \in$ 1,...,4.

The prior distribution, $p(\boldsymbol{\theta}) = p(\alpha_0, \alpha_1, \sigma_A, \sigma_B, \sigma_\epsilon, \mathbf{A}, \mathbf{B}, \mathbf{S})$, encompasses our prior knowledge or beliefs about the unknown parameters of interest and is composed of the individual prior distributions for each parameter. Prior distributions specify what we know about these parameters before any data has been collected and can be defined to incorporate realistic bounds, scientific judgment, or can cover a wide range of values to specify no prior knowledge.

For this analysis, we assume *a priori* that α_0 ~ Normal(-65, 10), which puts 95% of the prior probability between -84.6 and -45.4. For the slope, we assume α_1 is restricted to positive numbers because a negative slope is scientifically implausible and that α_1 follows a truncated

Normal(0, 10) distribution, which puts 95% of the prior probability between 0.31 and 22.42. These can be thought of as relatively flat prior distributions, spreading the prior probability between a wide range of numbers.

For the uncertainty parameters, σ_A, σ_B, and σ_ϵ, we assume half Student's *t*-distributions, bounded to be ≥ 0 since uncertainties must be positive, centered at zero, with a scale equal to 0.06, and with four degrees of freedom, which puts roughly 95% of the prior probability between 0 and 0.21. This distribution has a long tail, putting most of the prior weight on smaller values of these parameters but allowing for values that are larger if there is strong evidence in the data for larger uncertainties. We performed a sensitivity analysis, varying the size of the scales for these half Student's *t*-distributions, and found that the results reported below were not very sensitive to changes in these prior assumptions.

Once the prior distributions and the likelihood are defined, we can use Hamiltonian Monte Carlo, implemented via Stan [18] using the R [19] package "rstan" [20], to sample from the posterior distribution. From these samples we can estimate the mean of the posterior distribution, as well as 95% intervals that encompass our uncertainties for these parameter values.

Table 4. Transition Temperature as a Function of Heating Rate Calculated Using the Hierarchical Bayesian Model.

β^a (°C·min^{-1})	$t_\beta{}^b$ (°C)	$u(t_\beta)^c$ (°C)	LB^d (°C)	UB^e (°C)	$U(t_\beta)^f$ (°C)	k^g
0	-64.58	0.10	-64.78	-64.39	0.20	1.96
1	-64.55	0.09	-64.73	-64.38	0.17	1.96
3	-64.49	0.08	-64.65	-64.34	0.15	1.95
5	-64.44	0.09	-64.61	-64.26	0.17	1.98
10	-64.30	0.16	-64.56	-63.94	0.31	1.93

[a]Nominal heating rate. [b]Heating-rate specific transition temperature (posterior means) determined using the hierarchical Bayesian model (Eq. (1)). [c]Uncertainty for heating-rate specific transition temperature (posterior standard deviations) [d]Lower bounds of 95% credible intervals. [e]Upper bounds of 95% credible intervals. [f]Expanded uncertainty calculated from uncertainty bounds as (*UB* – LB)/2. [g]Expansion factor calculated as $k = U(t_\beta)/u(t_\beta)$.

Specifically, from the Bayesian analysis we sample from the posterior distributions of the model parameters, and we use posterior samples of the intercept and slope to calculate estimates and uncertainties of the transition temperature at different β values. In Table 4 we report estimated transition temperatures for each β of interest (i.e., posterior means, t_β), associated uncertainties (i.e., posterior standard deviations, $u(t_\beta)$), and the lower and upper bounds of 95% credible intervals (*LB* and *UB*, respectively). These bounds are calculated as the 2.5 and 97.5 percentiles of the posterior samples. Also included in Table 4 are the expanded

uncertainties ($U(t_\beta)$), calculated from the lower and upper bounds using (*UB* – *LB*)/2, and the expansion factor *k*, calculated as $U(t_\beta)/u(t_\beta)$. It should be noted that predictive checks were performed to validate the modeling approach used in this work, the results of which indicate that the proposed model is indeed reasonable (see Appendix A.5).

As was previously mentioned, the value that is of primary interest for a reference material is the transition temperature at thermal equilibrium (i.e., at β = 0 °C·min^{-1}). Table 4 shows that for RM 8103 that value is -64.58 °C; we refer to this as t_{tran} and it is the value that appears in Table 1 and is reported in the information sheet. Additionally, the t_β and $U(t_\beta)$ values reported in Table 4 at the other four heating rates are also included in the information sheet for RM 8103 for reference.

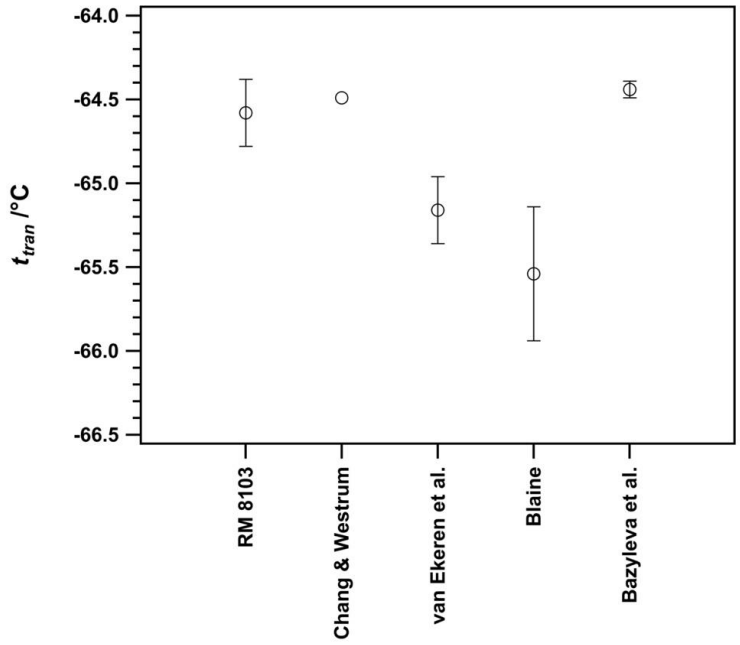

Figure 4. Comparison of transition temperature values. The reported value for RM 8103 is compared to values reported by Chang & Westrum [3, 4], van Ekeren et al. [21], Blaine [22], and Bazyleva et al. [23]. Error bars represent expanded (*k* ≈ 2) uncertainties. Expanded uncertainties for Blaine have been estimated from reported standard (*k* = 1) uncertainties [22] and no uncertainties were reported by Chang & Westrum [3, 4].

In Fig. 4 we have compared the transition temperature for RM 8103 with values found in the literature [3, 4, 21-23]. The values reported by Chang and Westrum [3, 4], van Ekeren et al. [21], and Bazyleva et al. [23] were all determined using adiabatic calorimetry. The transition temperature reported by Blaine [22] was based on an interlaboratory study which utilized DSC measurements and incorporated SRM 2225 as an internal standard; no additional details regarding instrument calibration or measurement protocols were provided. As is shown in Fig. 4, the transition temperature reported for RM 8103 agrees with the values reported by Chang and Westrum [3, 4] and Bazyleva et al. [23] within uncertainties, but not with those of van

Ekeren et al. [21] or Blaine [22]. The reason for this is unclear, although differences among the measured samples would seem to be a reasonable potential explanation. Chang and Westrum synthesized and purified the adamantane sample measured in their work and simply report that the resultant material was “pure adamantane” [3, 4]. All the other measured samples were purchased from commercial suppliers with a nominal purity of ≥ 99%, but only Bazyleva et al. subjected their sample to additional purification procedures; they report a final purity of 99.8% [23], the others do not report purity analysis results. Without additional information, it is not possible to draw any conclusions regarding the source of the discrepancies between the available literature values.

3.2. Enthalpy of Transition Results

In addition to the transition temperature, each of the resulting heat flow curves for the fifteen RM adamantane samples were analyzed to determine the measured enthalpy of transition (ΔH_{meas}). As is shown in the example in Fig. 3, the transition peak was integrated between the baseline endpoints (at -74 °C and -54 °C, for this example) to determine the area (mW·s), which was then divided by the sample mass to determine ΔH_{meas} (J·g^{-1}). The results for each individual replicate measurement are reported in Table A.4.1 of Appendix A.4. To aid in comparisons, the ΔH_{meas} results reported in Table A.4.1 are also shown in Fig. 5, plotted as a function of nominal heating rate. The sample source bottles are distinguished by six distinct markers and the bottle subsamples are differentiated by color. Once again, the greatest overall variability is observed at β = 10 °C·min^{-1}, but this is primarily attributed to a few outlying measurements. Outliers are also observed at β = 3 °C·min^{-1} and β = 5 °C·min^{-1}; if these points are ignored, the observed variabilities for the remaining points are actually similar at these three heating rates and the largest variability is then observed at β = 1 °C·min^{-1}.

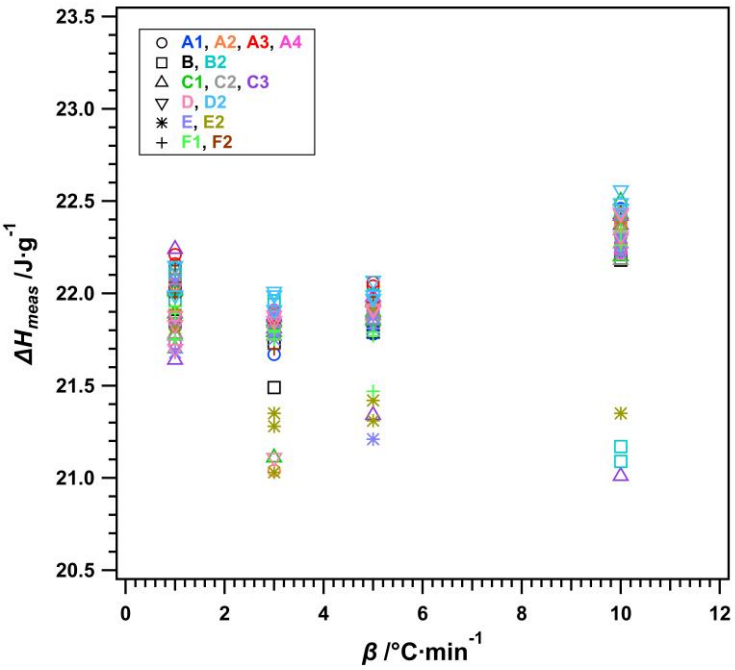

Figure 5. Replicate enthalpy of transition measurement results for fifteen RM 8103 samples plotted as a function of nominal heating rate. Samples sourced from six different 100 g bottles are plotted as distinct markers and bottle-specific subsamples are differentiated by color, as indicated by the included legend.

As was the case with the transition temperature, the goal is to use the measurement results shown in Fig. 5 to derive a single enthalpy of transition and its associated uncertainty for each of the measured heating rates (ΔH_β and $u(\Delta H_\beta)$, respectively) and, most importantly, at β = 0 °C·min^{-1}. Again, we have used a hierarchical Bayesian model [17] to achieve this goal. Specifically, for each measured enthalpy of transition value, we assume

$$\Delta H_{meas,ijk} = \alpha_0 + \alpha_1 \cdot \beta_{ijk} + A_i + B_{ij} + \epsilon_{ijk} + S_l \, . \quad (3)$$

Here, α_0 is the intercept, which corresponds to the value at β = 0 °C·min^{-1} (i.e., ΔH_{tran}), and α_1 is the slope. The "ijk" subscript indicates the k^{th} measurement for the j^{th} subsample within the i^{th} sample. In this work, i = 1,...,6 and j = 1,...,$n_{j(i)}$, with the number of subsamples, $n_{j(i)}$, within each sample varying from 1 to 4. A_i accounts for sample effects and is assumed to have a normal distribution with an expected value of zero and a variance of σ_A^2 (i.e., A_i ~ Normal(0, σ_A)). Similarly, B_{ij} accounts for subsample effects and B_{ij} ~ Normal(0, σ_B). Next, ϵ_{ijk} represents the measurement error due to random effects. To allow for possible outlying points, such as subsample 3 of sample C (e.g., sample C3 in Table 3) at β = 10 °C·min^{-1} (see Fig. 5), we assume ϵ_{ijk} has a Student's t-distribution with four degrees of freedom, an expected value of 0, and a scale selected such that its variance is equal to σ_ϵ^2. Finally, S_l represents the β-specific subsample effect with S_l ~ Normal(0, $\sigma_{S,l}$). Here, l indicates the associated nominal heating rate

(i.e., $l \in 1,...,4$ corresponding to β = 1, 3, 5, or 10 °C·min^{-1}). To determine $\sigma_{S,l}$ we calculate the uncertainty due to systematic effects, $u(\Delta H_{meas})$, and use the mean at each nominal β. The determination of $u(\Delta H_{meas})$ is discussed in detail in Sec. 4.2.

Once again, we use a Bayesian analysis to fit the model in Eq. (3). The analysis follows the approach described in detail in Sec. 3.1. Here, the observed data is defined as $\mathbf{x} = (\mathbf{H}, \boldsymbol{\beta}, \boldsymbol{\sigma_S})$ where $\mathbf{H}$ and $\boldsymbol{\beta}$ represent the $\Delta H_{meas,ijk}$ and β_{ijk} for all i, j, and k values and $\boldsymbol{\sigma_S}$ represents $\sigma_{S,l}$ for $l \in 1,...,4$. Here, we assume α_0 ~ Normal(22,10) (putting 95% of the prior probability between 2.4 and 41.6) and α_1 is positive and ~ Normal(0,10) (putting 95% of the prior probability between 0.31 and 22.42). For σ_A, σ_B, and σ_ϵ we assume half Student's t-distributions with four degrees of freedom, bounded to be ≥ 0, centered at zero, with a scale equal to 0.31 (putting 95% of the prior probability between 0.01 and 1.08).

In Table 5 we report estimated enthalpies of transition for each β of interest (i.e., posterior means, ΔH_β), associated uncertainties (i.e., posterior standard deviations, $u(\Delta H_\beta)$), and the lower and upper bounds of 95% credible intervals (*LB* and *UB*, respectively). These bounds are calculated as the 2.5 and 97.5 percentiles of the posterior samples. Also included in Table 5 are the expanded uncertainties ($U(\Delta H_\beta)$), calculated from the lower and upper bounds using (*UB* – *LB*)/2, and the expansion factor *k*, calculated as $U(\Delta H_\beta)/u(\Delta H_\beta)$. Again, the results of predictive checks indicate that the proposed model is indeed reasonable (see Appendix A.5).

As was previously mentioned, the value that is of primary interest for a reference material is the enthalpy of transition at thermal equilibrium (i.e., at β = 0 °C·min^{-1}). Table 5 shows that for RM 8103 the enthalpy of transition at β = 0 °C·min^{-1} is 21.64 J·g^{-1}; we refer to this as ΔH_{tran} and it is the value that appears in Table 1 and is reported in the information sheet. As with the transition temperatures, the ΔH_β and $U(\Delta H_\beta)$ values reported in Table 5 at the other four heating rates are also included in the information sheet for RM 8103 for reference.

Table 5. Enthalpy of Transition as a Function of Heating Rate Calculated Using the Hierarchical Bayesian Model.

β^a (°C·min^{-1})	$\Delta H_\beta{}^b$ (J·g^{-1})	$u(\Delta H_\beta)^c$ (J·g^{-1})	LB^d (J·g^{-1})	UB^e (J·g^{-1})	$U(\Delta H_\beta)^f$ (J·g^{-1})	k^g
0	21.64	0.18	21.27	21.95	0.34	1.92
1	21.70	0.15	21.40	21.96	0.28	1.93
3	21.82	0.10	21.62	22.00	0.19	1.94
5	21.93	0.09	21.76	22.10	0.17	1.95
10	22.23	0.21	21.87	22.67	0.40	1.90

[a]Nominal heating rate. [b]Heating-rate specific enthalpy of fusion (posterior means) determined using the hierarchical Bayesian model (Eq. (3)). [c]Uncertainty for heating-rate specific enthalpy of fusion (posterior standard deviations) [d]Lower bounds of 95% credible intervals. [e]Upper bounds of 95% credible intervals. [f]Expanded uncertainty calculated from uncertainty bounds as (*UB* – *LB*)/2. [g]Expansion factor calculated as $k = U(\Delta H_\beta)/u(\Delta H_\beta)$.

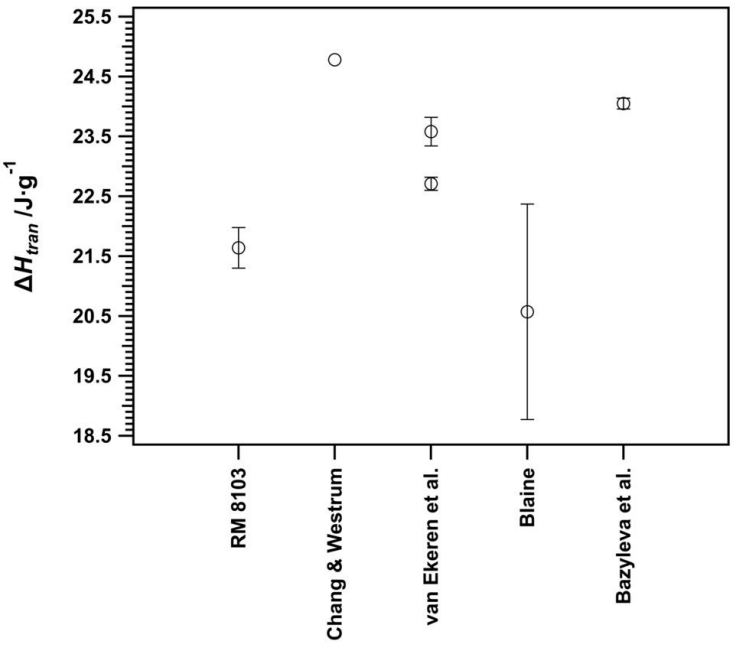

Figure 6. Comparison of enthalpy of transition values. The reported value for RM 8103 is compared to values reported by Chang & Westrum [3, 4], van Ekeren et al. [21], Blaine [22], and Bazyleva et al. [23]. Error bars represent expanded ($k \approx 2$) uncertainties. Expanded uncertainties for Blaine have been estimated from reported standard ($k = 1$) uncertainties [22] and no uncertainties were reported by Chang & Westrum [3, 4].

In Fig. 6 we have compared the enthalpy of transition for RM 8103 with values found in the literature [3, 4, 21-23]. Details concerning the literature sources were discussed in Sec. 3.1. Unlike with the transition temperatures (see Fig. 4), the enthalpy of transition reported for RM 8103 does not agree with the literature values within expanded uncertainties; the one exception is that of Blaine [22]. Interestingly, it is clear from Fig. 6 that none of the literature values agree with one another within reported uncertainties. As was previously discussed, differences between the measured adamantane samples could possibly explain the observed discrepancies but it is not possible to draw definitive conclusions without additional information (see Sec. 3.1). Perhaps a more likely explanation involves differences among the baselines utilized by the various authors. For both the Chang and Westrum value [3, 4] and the larger of the two van Ekeren et al. [21] values, a linear baseline was used. No details regarding the baseline were reported by Blaine but one of the included figures appears to indicate the use of a linear baseline [22]. However, the question has been raised whether such a choice is appropriate for an apparent first-order transition as is the case here [4, 23]. As a result, van Ekeren reports a second value obtained using an alternate baseline construction [21]. Similarly, Bazyleva et al. use two independent baselines for the low- and high-temperature crystals [23]. The sigmoidal tangent baseline used in this work does the same (see Sec. 3.1 and Appendix A.2). It is clear from previous work, as well as the uncertainty analysis performed in this work, that the choice of baseline can have a significant impact on the calculated enthalpy in

particular, but it is unclear whether it can fully account for the observed differences. However, while the disparities are disappointing, it does not nullify the usefulness of RM 8103 as a reference material for DSC calibration. The reported transition temperature and enthalpy values are not meant to be universally representative of adamantane; rather the values are representative of the single lot of material that makes up RM 8103.

4. Uncertainty Analysis

4.1. Transition Temperature Uncertainty Due to Systematic Effects

For transition temperature, measurement uncertainty can be attributed to both systematic and random effects. In this work, the hierarchical Bayesian model described in Sec. 3.1 accounts for both of these components. However, the uncertainty due to systematic effects must be supplied to the Bayesian model. Our approach to estimating this uncertainty is described here.

A single measurement of the transition temperature, t_{meas}, for a given sample at a single heating rate can be expressed as

$$t_{meas} = t_e + S\,, \tag{4}$$

where t_e is the estimated extrapolated onset temperature (°C), and S is the effect of the smoothing method on t_e (°C). The subject of curve smoothing will be discussed in greater detail in the following sections. The combined standard uncertainty, $u(t_{meas})$, can then be expressed as

$$u(t_{meas}) = \sqrt{u^2(t_e) + u^2(S)}\,, \tag{5}$$

where the uncertainty in the estimated extrapolated onset temperature, $u(t_e)$, can be estimated from simulation, and the uncertainty from curve smoothing, $u(S)$, is estimated from supporting analyses. The individual uncertainty components are discussed in more detail in Secs. 4.1.1 and 4.1.2. In this work, an averaged $u(t_{meas})$ was determined at each nominal β using data from a subset of the 15 adamantane samples; these averages were then used as model inputs (i.e., $\boldsymbol{\sigma_S}$). Specifically, the $\boldsymbol{\sigma_S}$ values used in this work were 0.124, 0.123, 0.171, and 0.310 °C at 1, 3, 5, and 10 °C·min^{-1}, respectively for transition temperature.

4.1.1. Uncertainty in Estimated Extrapolated Onset Temperature ($u(t_e)$)

We employed a simulation study to estimate the standard uncertainty in the estimated extrapolated onset temperature, $u(t_e)$. This allowed us to incorporate variability arising from the selection of the baseline endpoints, as well as individual heat flow and temperature measurements. To address the latter, we first had to estimate the standard uncertainties associated with the recorded heat flow and temperature signals. Heat flow uncertainties are discussed in detail in Sec. 4.2.1; temperature uncertainties are considered here.

As was previously discussed (see Sec. 2.2.1), when extrapolating to temperatures below the low-temperature calibrant, the measured temperature, t_{corr}, can be expressed as

$$t_{corr} = t_{rec} + corr\ , \tag{6}$$

where t_{rec} is the raw temperature recorded by the instrument and $corr$ is the applied calibration correction, which, in this work, is based on the mercury β-dependent calibration results shown in Table 2. The standard uncertainty in the measured temperature attributed to systematic effects, $u(t_{corr})$, can then be expressed as

$$u(t_{corr}) = \sqrt{u^2(t_{rec}) + u^2(corr)}\ . \tag{7}$$

The standard uncertainty in the raw temperature reading, $u(t_{rec})$, includes both the temperature accuracy ("acc") and precision ("$prec$"), and can be expressed as

$$u(t_{rec}) = \sqrt{u^2(acc) + u^2(prec)}\ . \tag{8}$$

The manufacturer estimates the accuracy and precision as 0.1 °C and 0.01 °C, respectively. If we assume that the manufacturer's specifications represent bounds for a uniform distribution, the corresponding standard uncertainties in accuracy ($u(acc)$) and precision ($u(prec)$) are estimated as

$$u(acc) = \frac{0.1}{\sqrt{3}} = 0.057735\ °\text{C} \tag{9}$$

and

$$u(prec) = \frac{0.01}{\sqrt{3}} = 0.0057735\ °\text{C}\ . \tag{10}$$

The second term in Eq. (7), the standard uncertainty in the calibration correction applied to the raw temperature signal, $u(corr)$, can be expressed as

$$u(corr) = \sqrt{u^2(t_{ref}) + u^2(\Delta t) + u^2(model)}\,, \tag{11}$$

where $u(t_{ref})$ is the standard uncertainty in the reference temperature, $u(\Delta t)$ is the standard uncertainty in the applied correction, and $u(model)$ is the standard uncertainty associated with the instrument's calibration model. As discussed in Sec. 2.2.1, the correction applied at temperatures below -38.8 °C is based solely upon the mercury calibration data; therefore, $u(t_{ref})$ is taken from the certificate of analysis for SRM 2225 and is equal to 0.015 °C [7]. Since the applied calibration correction is determined from an average of replicate measurements, $u(\Delta t)$ can be estimated as

$$u(\Delta t) = \frac{s_{t_{cal,avg}}}{\sqrt{n}}\,, \tag{12}$$

where $s_{t_{cal,avg}}$ is the standard deviation associated with the average melting temperature measured for mercury and n is number of calibration measurements averaged (10). The averaged melting temperature for both indium and mercury were previously reported in Table 2, for reference, the β-dependent values for mercury are reproduced in Table 6, along with the associated standard deviations.

Table 6. Averaged Measured Melting Temperatures from Ten Mercury Calibration Measurements as a Function of Heating Rate.

β^a (°C·min^{-1})	$t_{cal,avg}{}^b$ (°C)	$s_{t_{cal,avg}}{}^c$ (°C)
1	-37.845	0.005
3	-37.875	0.010
5	-37.907	0.013
10	-37.973	0.026

[a]Nominal heating rate. [b]Averaged measured melting temperature. [c]Standard deviation.

There is uncertainty associated with a calibration model that involves the application of a single correction value to all temperatures below -38.85 °C arising from both the assumed lack of temperature dependence at lower temperatures and the accuracy of the applied correction. Without additional low-temperature certified reference materials, it is difficult to reliably estimate the former. However, we can use the results of the aforementioned mercury check measurements (see Sec. 2.2.2) to estimate the latter. Comparing the measured melting

temperatures to the certified value [7], we found average offsets (Δ_{avg}) of 0.04 °C at 1 °C·min^{-1}, 0.07 °C at 3 °C·min^{-1}, 0.08 °C at 5 °C·min^{-1}, and 0.33 °C at 10 °C·min^{-1}. If we assume that these values represent the bounds of a uniform distribution, the standard uncertainty in the calibration model, $u(model)$, can be estimated as

$$u(model) = \frac{\Delta_{avg}}{\sqrt{3}}. \tag{13}$$

Using Eq. (7), $u(t_{corr})$ was calculated as a function of time for each of the measured temperature curves; these uncertainty values defined boundaries for the subsequent simulations. Specifically, customized code, developed using Igor Pro data analysis software [24], was used to construct a new temperature curve by applying a single randomly assigned error to each data point; the error was selected from within the bounds of a uniform (-a, a) distribution with

$$a = u(t_{corr}) \cdot \sqrt{3}\ . \tag{14}$$

Similarly, a simulated heat flow curve is generated by applying a randomly assigned error which was selected from within the limits of a uniform distribution using an expression analogous to Eq. (14). Next, the simulated temperature and heat flow curves are smoothed, and an inflectional tangent line constructed. Since this step involves the use of the first and second numerical derivatives, some degree of smoothing is required; without it, the resulting derivatives are too noisy to reliably determine an inflection point. For these simulations, only the "best" smoothing method was employed, which was determined from prior supporting analyses. Specifically, using the data generated during separate smoothing simulations (see Sec. 4.1.2), we determined that the boxcar smoothing method produced optimal results; the corresponding β-specific smoothing parameters are shown in Table 7 for reference.

Table 7. Optimal Boxcar Smoothing Parameters as a Function of Heating Rate.

β^a (°C·min^{-1})	Box Width	# Passes
1	11	40
3	7	20
5	5	10
10	5	5

[a]Nominal heating rate.

To simulate baseline variability, endpoint pairs defining the peak's start and stop were randomly selected from defined intervals that varied depending on heating rate. These endpoints were then used to construct a new baseline for the simulated heat flow curve. As was previously mentioned, a sigmoidal tangent baseline was used for the RM 8103 measurements (see Sec. 3.1 and Appendix A.2). However, for the sake of computational simplicity, the simulations discussed here utilized a stepped baseline where two separate linear baselines are constructed on either side of the transition peak and each extrapolated to meet at the peak minimum (see Fig. 7). Previous work has shown that the stepped baseline yields results that are reasonably similar to those obtained with a sigmoidal tangent baseline and, therefore, is suitable for use in simulations.

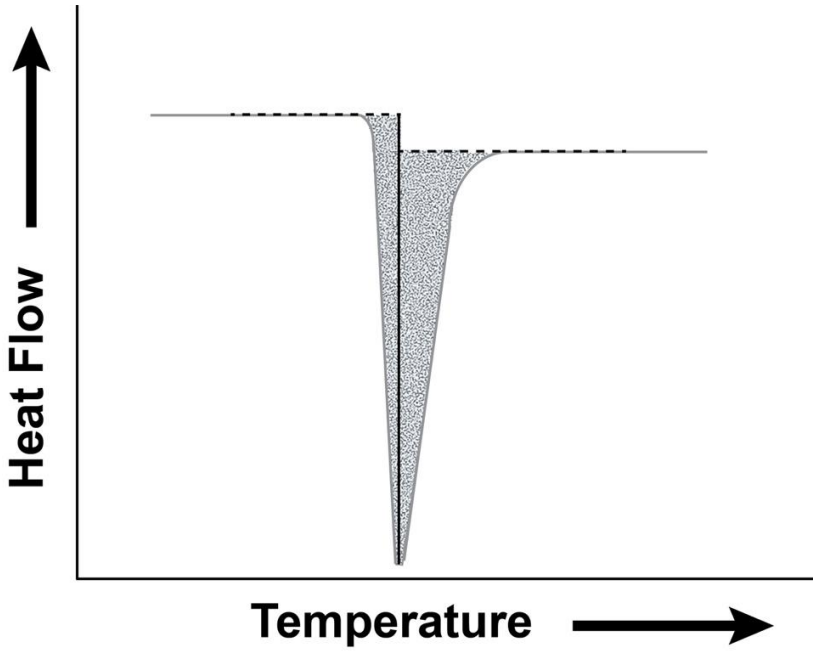

Figure 7. Schematic representation of stepped baseline used in uncertainty simulations. The gray line represents a theoretical melting curve. The dashed black lines represent extrapolated linear baselines constructed on either side of the peak. The solid black line represents the peak minimum and marks the endpoint for the extrapolated baselines. The shaded gray represents the integrated peak area.

Using the simulated inflectional tangent line and stepped baseline, a new t_e was calculated. This process was repeated 10,000 times and the overall mean and standard deviation determined, with the standard deviation representing the uncertainty in the extrapolated onset temperature, $u(t_e)$. Figure 8 shows a sample histogram displaying the results of the extrapolated onset temperature simulations for a single replicate measurement of the A4 sample at 1 °C·min^{-1}. In this example, the $u(t_e)$ is 0.064 °C. A separate determination of $u(t_e)$ was made for each replicate measurement, at each heating rate, for four of the fifteen RM adamantane samples. The four samples (B, A4, E2, and D2) were chosen to represent the full

range of measured sample masses. The results from these four samples were combined with corresponding $u(S)$ values (Sec. 4.1.2) to determine an average $u(t_{meas})$ at each of the four heating rates.

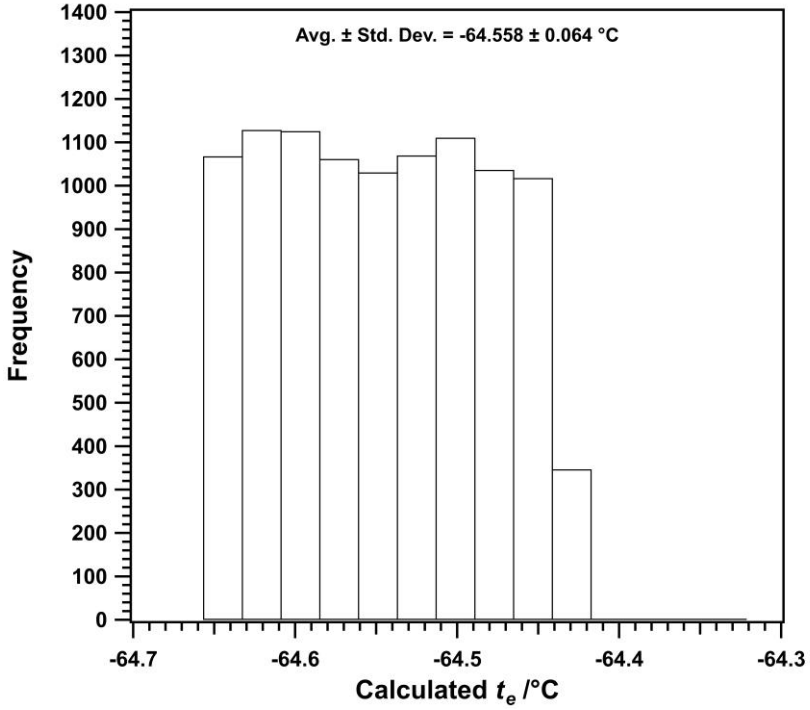

Figure 8. Sample histogram for extrapolated onset temperature simulations. Shown are the results for a single replicate measurement of the A4 sample at 1 °C·min^{-1}. The resulting average and associated standard deviation are displayed. The estimated uncertainty in the measured extrapolated onset temperature, $u(t_e)$, is set equal to the standard deviation.

4.1.2. Uncertainty from Smoothing ($u(S)$)

To estimate the standard uncertainty introduced by smoothing, $u(S)$, we employed another simulation study utilizing custom Igor Pro code [24]. For this study, no errors were applied to the measured temperature and heat flow curves, and the baseline endpoints remained fixed at the values used in the original analysis. As was described in the previous section (Sec. 4.1.1), for simplicity, a stepped baseline (such as that depicted in Fig. 7) was used in these simulations. Here, the only parameter being perturbed in each of the simulation runs was the type and degree of smoothing applied prior to the determination of the inflection point that is used to construct the inflectional tangent line. Specifically, for each simulation run, the type of smoothing is randomly selected from three different methods: (1) binomial, (2) boxcar, and (3) Savitzky-Golay. For a given method, the associated parameters are randomly assigned from within allowed limits; for binomial smoothing the allowed number of passes ranged from 1 to 1000, for boxcar smoothing the box width was limited to odd values between 3 and 25 and the allowed number of passes ranged from 1 to 100, and for Savitzky-Golay smoothing the number of points were limited to odd values between 5 and 25 and the allowed order was either 2 or 4.

Simulations were run for all replicate measurements of three RM adamantane samples at all four heating rates. The three samples chosen (B, A4, and D2) together cover the full range of sample masses measured in this work. Once again, a total of 10,000 extrapolated onset temperatures were simulated for each sample and the overall mean and standard deviation determined. In addition, the minimum and maximum observed t_e were determined. Figure 9 shows a sample histogram displaying the results of the smoothing simulations for a single replicate measurement of the A4 sample at 1 °C·min^{-1}. In this example, the minimum t_e is -64.585 °C and the maximum t_e is -64.334 °C. A separate determination of the minimum and maximum t_e was made for each replicate measurement, at each heating rate, for the three selected RM adamantane samples.

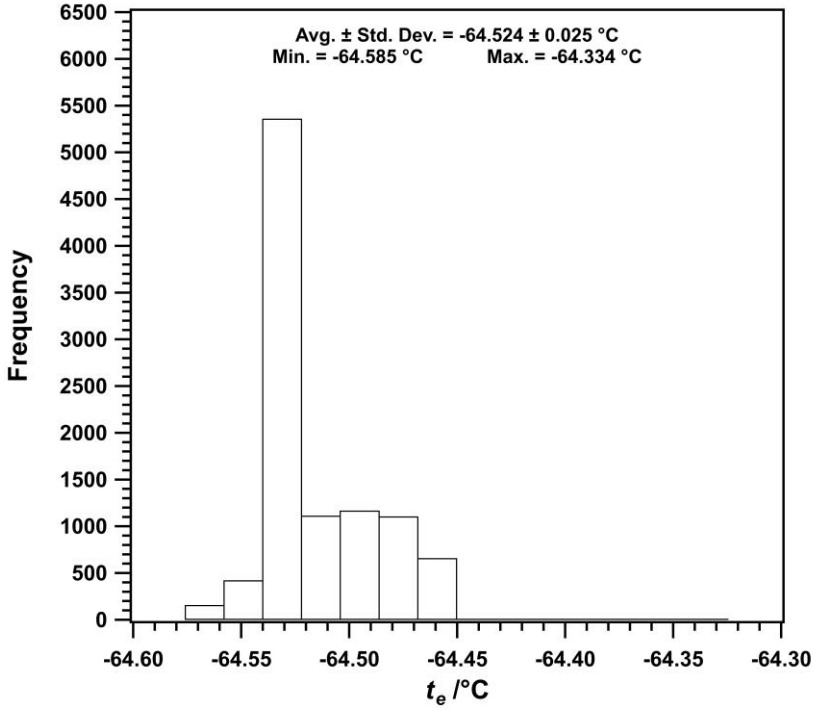

Figure 9. Sample histogram for smoothing simulations. Shown are the results for a single replicate measurement of the A4 sample at 1 °C·min^{-1}. The resulting average and associated standard deviation are displayed, along with the minimum and maximum observed extrapolated onset temperatures. The minima and maxima are used to estimate the uncertainty from smoothing, $u(S)$, as described in the text.

If we assume the observed minima and maxima represent the bounds of a uniform distribution, the standard uncertainty from smoothing, $u(S)$ can be estimated using

$$u(S) = \frac{(\max - \min)}{\sqrt{12}}. \quad (15)$$

For each heating rate, we selected the largest of the resulting nine values (i.e., three samples with three replicate measurements each) as a conservative estimate of $u(S)$. The β-dependent results are shown in Table 8 for reference.

Table 8. Estimate of Uncertainty from Smoothing, $u(S)$, as a Function of Heating Rate.

β^a (°C·min^{-1})	$u(S)$ (°C)
1	0.106
3	0.100
5	0.153
10	0.236

[a]Nominal heating rate.

4.2. Enthalpy of Transition Uncertainty Due to Systematic Effects

The hierarchical Bayesian model described in Sec. 3.2 for the enthalpy of transition accounts for measurement uncertainties from both systematic and random effects. Here we describe our approach to estimating the systematic uncertainty that must be supplied to the model.

A single measurement of the enthalpy of transition, ΔH_{meas}, for a given sample at a single heating rate can be expressed as

$$\Delta H_{meas} = \frac{x}{m} , \tag{16}$$

where x is the integrated peak area (mW·s), and m is the sample mass (mg). The combined standard uncertainty attributed to systematic effects, $u(\Delta H_{meas})$, can then be expressed as

$$u(\Delta H_{meas}) = \sqrt{\left(\frac{1}{m}\right)^2 u^2(x) + \left(\frac{-x}{m^2}\right)^2 u^2(m)} , \tag{17}$$

where the uncertainty in the integrated peak area, $u(x)$, can be estimated from simulation, and the uncertainty in mass, $u(m)$, is estimated at 0.003 mg. The individual uncertainty components are discussed in more detail in Secs. 4.2.1 and 4.2.2. In this work, an averaged $u(\Delta H_{meas})$ was determined at each nominal β using data from a subset of the 15 adamantane samples; these averages were then used as model inputs (i.e., $\boldsymbol{\sigma_S}$). Specifically, the $\boldsymbol{\sigma_S}$ values

used in this work were 0.305, 0.145, 0.101, and 0.320 J·g^{-1} at 1, 3, 5, and 10 °C·min^{-1}, respectively, for enthalpy of transition.

4.2.1. Uncertainty in Integrated Peak Area ($u(x)$)

As was the case with the uncertainty in the transition temperature (see Sec. 4.1.1), we employed a simulation study to estimate the standard uncertainty in the integrated peak area, $u(x)$. This allowed us to incorporate variability arising from the selection of the baseline endpoints, as well as individual heat flow measurements. We assumed that time was measured without statistically significant error and, therefore, did not incorporate variability from those measurements in our simulations.

To address heat flow measurement variability, we first had to estimate the uncertainty associated with the heat flow signal that is recorded by the instrument. Recorded heat flow, HF_{record}, can be expressed as

$$HF_{record} = K_q \cdot HF_{raw} \ , \tag{18}$$

where K_q is an (unitless) enthalpy calibration coefficient and HF_{raw} is the raw (i.e., uncalibrated) heat flow signal (mW). The standard uncertainty in the recorded heat flow, $u(HF_{record})$, can then be expressed as

$$u(HF_{record}) = \sqrt{(HF_{\text{raw}})^2 u^2(K_q) \ + \ (K_q)^2 u^2(HF_{\text{raw}})} \ . \tag{19}$$

As was previously discussed (Sec. 2.2.1), K_q was obtained by measuring materials with known transition enthalpies and calculating the ratio of the reference transition enthalpy, ΔH_{ref} (J·g^{-1}), to the experimentally determined transition enthalpy, ΔH_{cal} (J·g^{-1}):

$$K_q = \frac{\Delta H_{ref}}{\Delta H_{cal}} + C \ . \tag{20}$$

Here, C represents an additional systematic uncertainty contribution associated with the enthalpy calibration. The standard uncertainty in K_q, $u(K_q)$, can then be expressed as

$$u(K_q) = \sqrt{\left[\frac{\partial K_q}{\partial \Delta H_{ref}}\right]^2 u^2(\Delta H_{ref}) + \left[\frac{\partial K_q}{\partial \Delta H_{cal,avg}}\right]^2 u^2(\Delta H_{cal,avg}) + u^2(C)}\,. \quad (21)$$

In Eq. (21), the two partial derivatives are defined as follows:

$$\frac{\partial K_q}{\partial \Delta H_{ref}} = \frac{1}{\Delta H_{cal,avg}} \text{ and} \quad (22)$$

$$\frac{\partial K_q}{\partial \Delta H_{cal,avg}} = -\frac{\Delta H_{ref}}{(\Delta H_{cal,avg})^2}\,. \quad (23)$$

The calibration certificate for the indium certified reference material used in this work reports an expanded (k = 2) uncertainty of 0.06 J·g^{-1} [6], therefore the uncertainty associated with the reference enthalpy, $u(\Delta H_{ref})$, is 0.03 J·g^{-1}. The random uncertainty associated with the enthalpy calibration measurements, $u(\Delta H_{cal,avg})$, can be defined as

$$u(\Delta H_{cal,avg}) = \frac{s_{\Delta H_{cal,avg}}}{\sqrt{10}}\,, \quad (24)$$

where $\Delta H_{cal,avg}$ is the average enthalpy of fusion and $s_{\Delta H_{cal,avg}}$ is the sample standard deviation (J·g^{-1}) of the 10 enthalpy calibration measurements discussed in Sec. 2.2.1. The β-specific values used in the above equations are shown in Table 2 for K_q and in Table 9 for $\Delta H_{cal,avg}$, and $s_{\Delta H_{cal,avg}}$.

The final term in Eq. (21) was estimated by comparing the results of the mercury check measurements (Sec. 2.2.2) with the certified enthalpy value [7]. Based on those comparisons, we conservatively estimate that the enthalpy calibration contributes an additional systematic error to the resulting K_q values, the value of which depends on the heating rate. Assuming this error represents the bounds on a uniform distribution, the standard uncertainty from the enthalpy calibration, $u(C)$, is then expressed as

$$u(C) = \frac{(p/100)}{\sqrt{3}}\,, \quad (25)$$

where p is the percent error; p is estimated to be 2.2% at 1 °C·min^{-1}, 1.1% at 3 °C·min^{-1}, 0.7% at 5 °C·min^{-1}, and 2.5% at 10 °C·min^{-1}.

Table 9. Averaged Measured Enthalpy of Fusion from Ten Indium Calibration Measurements as a Function of Heating Rate.

β^a (°C·min^{-1})	$\Delta H_{cal,avg}{}^b$ (J·g^{-1})	$s_{\Delta H_{cal,avg}}{}^c$ (J·g^{-1})
1	27.209	0.093
3	27.182	0.082
5	27.151	0.094
10	27.169	0.125

[a]Nominal heating rate. [b]Averaged measured enthalpy of fusion. [c]Standard deviation.

Finally, in Eq. (19), the uncertainty in the raw heat flow signal, $u(HF_{raw})$, is estimated by converting the manufacturer's "baseline reproducibility" of 0.01 mW to a standard uncertainty based on the assumption that the manufacturer's specifications represent bounds for a uniform distribution:

$$u(HF_{\text{raw}}) = \frac{0.01}{\sqrt{3}} = 0.0057735 \text{ mW} . \quad (26)$$

Using Eq. (19), $u(HF_{record})$ was calculated as a function of time for each of the measured heat flow curves; these uncertainty values defined boundaries for the subsequent simulations. As was previously described (Sec. 4.1.1), customized Igor Pro code [24] was used to construct a new heat flow curve by applying a single randomly assigned error to the measured curve where the error was selected from within the limits of a uniform distribution using an expression analogous to Eq. (14).

To simulate baseline variability, new endpoint pairs defining the peak's start and stop were randomly selected and a stepped baseline constructed for the simulated heat flow curve (e.g., Fig. 7); the peak was integrated, and a new ΔH_{meas} was calculated. Note that, in contrast to the temperature simulations (Sec. 4.1.1), no smoothing was applied to the simulated enthalpy curves. This process was repeated 10,000 times and the overall mean and standard deviation determined, with the standard deviation representing the uncertainty in the integrated peak area, $u(x)$. Figure 10 shows a sample histogram displaying the results of the enthalpy simulations for a single replicate measurement of the A4 sample at 1 °C·min^{-1}. In this example, the estimated uncertainty in the measured peak area ($u(x)$) is 2.560 mW·s. A separate determination of $u(x)$ was made for each replicate measurement, at each heating rate, for four

of the fifteen RM adamantane samples (B, A4, E2, and D2). The results from these four samples were combined with corresponding $u(m)$ values (Sec. 4.2.2) to determine an average $u(\Delta H_{meas})$ at each of the four heating rates.

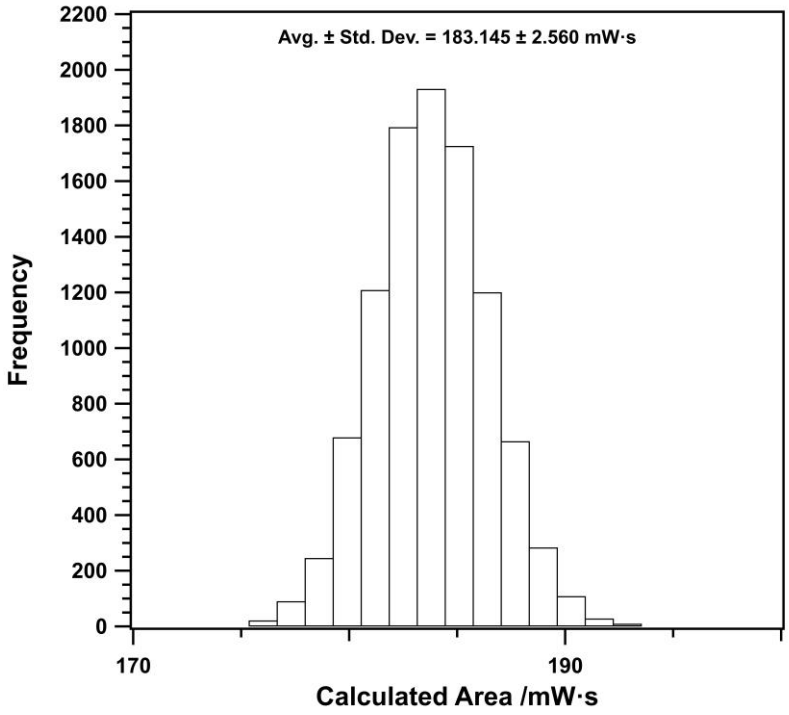

Figure 10. Sample histogram for enthalpy simulations. Shown are the results for a single replicate measurement of the A4 sample at 1 °C·min^{-1}. The resulting average and associated standard deviation are displayed. The estimated uncertainty in the measured peak area, $u(x)$, is set equal to the standard deviation.

4.2.2. Uncertainty in Sample Mass ($u(m)$)

We have estimated the standard uncertainty in sample mass, $u(m)$, as

$$u(m) = \sqrt{u_A^2 + u_B^2}\,, \tag{27}$$

where u_A denotes a type A uncertainty evaluation and u_B denotes a type B uncertainty evaluation [25, 26]. In this work,

$$u_A = \frac{s_p}{\sqrt{n}}\,, \tag{28}$$

where s_p is the standard deviation of the measurement process (mg), which is determined from a balance control chart, and n is the number of replicate sample weighings [12]. The value of u_B was estimated as

$$u_B = \sqrt{u_r^2 + u_{buoy}^2 + u_s^2}\,. \tag{29}$$

The first term, u_r, is the combined standard uncertainty of all reference masses utilized in the ABBA weighing scheme (mg), which are combined as a simple sum [27]. The second term, u_{buoy}, is the uncertainty associated with the applied air buoyancy correction (mg), which was estimated as

$$u_{buoy} = \sqrt{(V_x - V_r)^2 \cdot u_{\rho_{air}}^2 + \rho_{air}^2 \cdot \left(u_{V_x} - u_{V_r}\right)^2}\,. \tag{30}$$

Here, V_x and V_r are the volumes of the sample and reference pans, respectively, and u_{V_x} and u_{V_r} are the corresponding standard uncertainties in the pan volumes. The two remaining terms refer to the calculated air density (ρ_{air}) and its standard uncertainty ($u_{\rho_{air}}$). In this work, the standard uncertainties in sample and reference pan volumes are equivalent, reducing Eq. (30) to a function of pan volumes and the uncertainty in air density. The uncertainty in calculated air density is calculated as

$$u_{\rho_{air}} = \rho_{air} \cdot \sqrt{u_T^2 + u_{RH}^2 + u_p^2 + u_{eq}^2}\,, \tag{31}$$

where u_T, u_{RH}, u_p, and u_{eq} are the relative standard uncertainties associated with the measurements of room temperature, relative humidity, and pressure, as well as the equation used in the air density calculation [28].

The final term in Eq. (29), u_s, is the uncertainty arising from balance sensitivity (mg), which was estimated using an average of individual sensitivity values determined as part of the employed weighing scheme [12]. In this work, $u(m)$ was estimated to be 0.003 mg for all measured samples. The values for each of the primary uncertainty components are summarized in Table 10.

Table 10. Estimated Uncertainty in Sample Mass.

Component	$u(z)^a$ (mg)
u_A	0.001080
u_r	0.000750
u_{buoy}	0.000004
u_s	0.002044
u_B	0.002431
$u(m)^b$	0.003

[a]Standard (k = 1) uncertainty estimate for the corresponding component. [b]Combined standard uncertainty in sample mass calculated using Eq. (27).

5. Conclusions

The evaluation of RM 8103 has shown that the material is of high purity (≥ 99.9%) and is suitable for use as a temperature and enthalpy reference standard for the low-temperature calibration of DSCs. The reported transition temperature is (-64.58 ± 0.20) °C and enthalpy of transition is (21.64 ± 0.34) $J \cdot g^{-1}$. Both values were determined via DSC measurements of 15 samples randomly sourced from six 100 g bottles of commercially acquired adamantane, all from a single lot of material. The DSC employed in this work was calibrated for temperature and enthalpy using certified reference materials obtained from two national metrology institutes, NIST and PTB. The NIST reference material was certified via adiabatic calorimetry measurements [7], while the PTB reference material was certified via comparison with a fixed-point standard and measurements using a modified Tian-Calvet calorimeter for temperature and enthalpy, respectively [6].

References

[1] Hakvoort G (1994) DSC Calibration Below 0 °C. *J Therm Anal* 41:1551-1555.
[2] Price DM (1995) Temperature Calibration of Differential Scanning Calorimeters. *J Therm Anal* 45:1285-1296.
[3] Chang S-S, Westrum EF (1960) Heat Capacities and Thermodynamic Properties of Globular Molecules. I. Adamantane and Hexamethylenetetramine. *J Phys Chem* 64:1547-1551.
[4] Westrum EF (1961) The Thermophysical Properties of Three Globular Molecules. *J Phys Chem Solids* 18:83-85.
[5] Rosasco GJ, Whetstone JR, Watters RL (2005) Certificate of Analysis - Standard Reference Material 2232 (National Institute of Standards and Technology, Gaithersburg, MD).
[6] Sarge S, Hansen D (2018) Calibration Certificate - Indium Certified Reference Material (Physikalisch-Technische Bundesanstalt, Braunschweig, Germany).
[7] Rasberry SD (1989) Certificate of Analysis - Standard Reference Material 2225 (National Institute of Standards and Technology, Gaithersburg, MD).
[8] Preston-Thomas H (1990) The International Temperature Scale of 1990 (ITS-90). *Metrologia* 27:3-10.
[9] Boerio-Goates J, Callanan JE (1992) Differential Thermal Methods. *Physical Methods of Chemistry, Volume VI: Determination of Thermodynamic Properties*, eds Rossiter BW & Baetzold RC (John Wiley & Sons, New York, NY), Chapter 8, 2nd Ed., pp 621-717.
[10] Gmelin E, Sarge SM (1995) Calibration of Differential Scanning Calorimeters. *Pure Appl Chem* 67:1789-1800.
[11] Höhne GWH, Hemminger W, Flammersheim HJ (1996) *Differential Scanning Calorimetry: An Introduction for Practitioners* (Springer-Verlag, Berlin, Germany).
[12] Harris GL (2019) Selected Laboratory and Measurement Practices and Procedures to Support Basic Mass Calibrations (National Institute of Standards and Technology, Gaithersburg, MD), NISTIR 6969.
[13] Fortin TJ, Bruno TJ, Lovestead TM (2023) Comparison of Heat Capacity Measurements of Alternative and Conventional Aviation Fuels. *Int J Thermophys* 44:5.
[14] Della Gatta G, Richardson MJ, Sarge SM, Stølen S (2006) Standards, Calibration, and Guidelines in Microcalorimetry Part 2. Calibration Standards for Differential Scanning Calorimetry. *Pure Appl Chem* 78:1455-1476.
[15] Sarge SM, Gmelin E, Höhne GWH, Cammenga HK, Hemminger W, Eysel W (1994) The Caloric Calibration of Scanning Calorimeters. *Thermochim Acta* 247:129-168.
[16] ASTM International (2018) Standard Test Method for Temperature Calibration of Differential Scanning Calorimeters and Differential Thermal Analyzers (ASTM International, West Conshohocken, PA), ASTM E967-18.
[17] Gelman A, Carlin JB, Stern HS, Dunson DB, Vehtari A, Rubin DB (2014) *Bayesian Data Analysis* (CRC Press, Boca Raton, FL), 3rd Ed.
[18] Stan Development Team (2022) Stan Modeling Language Users Guide and Reference Manual, 2.32. https://mc-stan.org
[19] R Core Team (2023) R: A Language and Environment for Statistical Computing (R Foundation for Statistical Computing, Vienna, Austria). https://www.R-project.org
[20] Stan Development Team (2022) RStan: The R interface to Stan, 2.21.7. https://mc-stan.org

[21] van Ekeren PJ, van Genderen ACG, van den Berg GJK (2006) Redetermination of the Thermodynamic Properties of the Solid-Solid Transition of Adamantane by Adiabatic Calorimetry to Investigate the Suitability as a Reference Material for Low-Temperature DSC Calibration. *Thermochim Acta* 446:33-35.
[22] Blaine RL (2008) Adamantane - A New Certified and Traceable Reference Material for Subambient DSC Temperature and Enthalpy Calibration on Heating and Cooling (TA Instruments, New Castle, DE), Application Note TA372.
[23] Bazyleva AB, Blokhin AV, Kabo GJ, Charapennikau MB, Emel'yanenko VN, Verevkin SP, Diky V (2011) Thermodynamic Properties of Adamantane Revisited. *J Phys Chem B* 115:10064-10072.
[24] Igor Pro Development Team (2022) Igor Pro (WaveMetrics Inc., Lake Oswego, OR), 8.04. https://wavemetrics.com
[25] Kochsiek M, Gläser M (1999) *Comprehensive Mass Metrology* (Wiley-VCH, Berlin, Germany).
[26] BIPM (2008) Evaluation of Measurement Data - Guide to the Expression of Uncertainty in Measurement. (International Bureau of Weights and Measures (BIPM), Joint Committee for Guides in Metrology (JCGM), Sèvres, France), JCGM 100:2008.
[27] Schwartz R (2000) Mass Determination with Balances. *Comprehensive Mass Metrology*, eds Kochsiek M & Gläser M (Wiley-VCH, Berlin, Germany), Chapter 3.4, pp 232-295.
[28] Picard A, Davis RS, Gläser M, Fujii K (2008) Revised Formula for the Density of Moist Air (CIPM-2007). *Metrologia* 45:149-155.
[29] TA Instruments (2002) *Universal Analysis: Operator's Manual* (TA Instruments, New Castle, DE).
[30] van der Plaats G (1984) A Theoretical Evaluation of a Heat-Flow Differential Scanning Calorimeter. *Thermochim Acta* 72:77-82.

Appendix A. Supplemental Materials

A.1. Sample Analysis

Purity of the adamantane RM material was independently analyzed via GC-MS by NIST colleagues within the Applied Chemicals and Materials Division of the Material Measurement Laboratory. Results indicate a purity of (100.0 ± 0.1) % (see Fig. A.1.1).

UNITED STATES DEPARTMENT OF COMMERCE
National Institute of Standards and Technology
325 Broadway
Boulder, Colorado 80305-3337

647.07
Tel: 303-497-3553
Fax: 303-497-6682
Email: megan.harries@nist.gov

December 10, 2020

To: Tara Fortin, Research Chemist, Div. 647.08

From: Megan Harries, Postdoctoral Associate, Div. 647.07

Subject: Purity analysis of adamantane samples

Six samples of adamantane were presented for an assessment of their purity using gas chromatography and single quadrupole mass spectrometry (GC-MS). The samples were designated with the letters A-F. To prepare each sample for analysis, about 5 mg of the sample was dissolved in approximately 1.5 mL acetone. A 30 m capillary column of 5 % phenyl-95 %-dimethyl polysiloxane having a thickness of 0.25 µm and an internal diameter of 250 µm was used. The samples were injected in triplicate by an autosampler into a split/splitless injector operated in split mode with a split ratio of 10:1. The injector was held at a temperature of 275 °C and a constant flow rate of 1.0 mL/min. The oven temperature was initially 70 °C held for 13 min; it ramped at 20 °C/min to 275 °C. The ion source temperature was 230 °C and the quadrupole temperature was 150 °C. Mass spectra were collected from 33 to 400 relative molecular mass (RMM) units. Spectral peaks were interpreted with guidance from the NIST/EPA/NIH Mass Spectral Database.[1]

The analysis did not identify any impurities in any of the samples, resulting in a calculated purity of 100 % ± 0.1 %. The uncertainty was determined based on the instrument's limit of detection. Because of a necessary solvent delay of 2 min, any impurity eluting with a retention time of 0-2 min was not detected. Water as an impurity, or any impurity with a molecular weight below $3.3*10^{-2}$ kg/mol, was not detected.

Figure 1. A representative chromatogram (analysis of Sample C). The peak at 11.2 min is adamantane.

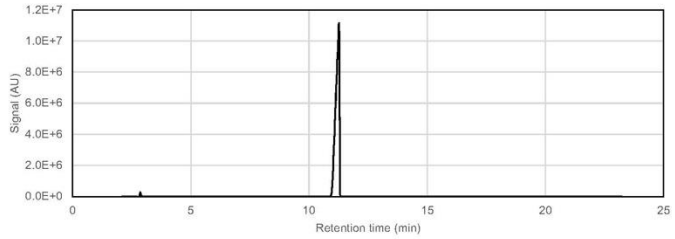

1. NIST/EPA/NIH Mass Spectral Database, SRD, 2011b. SRD Program, National Institute of Standards and Technology, Gaithersburg, MD, 2013.

Figure A.1.1. Results of GC-MS purity analysis.

UNITED STATES DEPARTMENT OF COMMERCE
National Institute of Standards and Technology
325 Broadway
Boulder, Colorado 80305-3337

647.07
Tel: 303-497-5207
Email: jason.widegren@nist.gov

January 8, 2021

To: Tara Fortin, Tara Lovestead
From: Jason Widegren
Subject: Analysis of six adamantane samples by Karl Fischer titration

Before the adamantane samples were analyzed, a control sample was analyzed for water content by coulometric Karl Fischer (KF) titration in order to check instrument performance and repeatability. The general procedure for this KF measurement is given in ASTM Standard Test Method E 1064-00. The control sample was a commercial water concentration standard (Hydranal®-Water Standard 0.1, Lot# SZBG039BV, distributed by Fluka Analytical in 5 mL glass ampules) with a water concentration of (104 ± 1) µg/g (at k = 2) according to the manufacturer. Five replicate analyses, each with a newly opened ampule, were made. The mass of injected standard ranged from 3.3682 g to 3.8959 g. By KF titration, the average water concentration from the five replicates was 105.6 µg/g (with a standard deviation of 0.9 µg/g). For well-behaved liquid samples, the standard uncertainty of KF titrations in this concentration range is 10 µg/g. Therefore, we found the water concentration in the standard to be (105.6 − 10) µg/g, which is consistent with the manufacturer's uncertainty statement.

Six samples of adamantane were presented in 20-mL glass scintillation vials and were labeled with letters from A to F. Each sample was analyzed for water content by coulometric KF titration. As for the adamantane samples analyzed in July 2019, Hydranal Coulomat AG-H was used as the KF reagent for these new titrations to aid with solubility. Adamantane still has a limited solubility in this reagent, so the reagent had to be changed after about 1 g (total) of adamantane had been titrated to ensure complete dissolution during the titration period. Even with the Coulomat AG-H, a 5-minute delay was used between sample introduction and sample titration to allow the sample to fully dissolve. A minimum of three replicate titrations were done for each sample of adamantane.

Since adamantane is a solid, it cannot be introduced into the titrator through the septum with a syringe (which is the "normal" procedure). Instead, (0.1 to 0.2) g of an adamantane sample was weighed into an aluminum boat. The septum was removed from the sample introduction port, the sample was poured into the titration vessel, the septum was replaced, and the aluminum boat was re-weighed (the mass of sample introduced into the titrator was determined by difference). This procedure briefly exposes the inside of the titration vessel to ambient air, which can introduce a significant amount of moisture into the device. To account for this additional source of moisture, six "blank" experiments were performed in which an empty aluminum boat was used to simulate the introduction of sample (Table 1). On average, 9.1 µg of water was introduced during a blank experiment (with a standard deviation of 2.3 µg of water). The average result for the blank experiments was subtracted from the results of each adamantane analysis before calculating the water concentration. The standard deviation in the blank titrations was used to determine the uncertainty caused by the sample introduction method.

Table 1. Six "blank" experiments were performed over the course of the adamantane titrations. The absolute mass of water detected in each blank experiment is given.

blank titration	H_2O / µg
1	10.8
2	11.7
3	5.5
4	11.2
5	8.1
6	7.4
Average	**9.1**
Std. Dev.	**2.3**

The results of KF titrations for the six adamantane samples are given in Table 2. The average water concentration for each sample, and the associated combined standard measurement uncertainty (u_c), are shown in bold, blue typeface. The combined standard uncertainty was calculated by quadrature addition of the scatter in replicate determinations (as represented by the standard deviation), the uncertainty in the blank subtraction (u_{blank}), and the average measured offset from the water concentration of the standard solution (u_{offset}, calculated as a percentage of the measured value). The relative uncertainty in water concentration is higher for these for these adamantane samples than for titrations done on liquid-phase samples. I believe that the primary reason for this is the sample introduction technique, which introduces a poorly controlled amount of ambient moisture and severely limits the sample size. At the k = 1 level, some of the uncertainty intervals for the six adamantane samples do not overlap; however, at the k = 2 level the uncertainty intervals for all six samples do overlap (Figure 1).

As can be seen in Figure 1, the measurement uncertainty was smaller for these new titrations than for the ones done in July 2019. The most likely explanation for this is the time of year for the titrations. The low humidity in December (compared to July) means that a smaller, less variable amount of atmospheric moisture is introduced into the titrator with the sample. For the new titrations, the water concentration is systematically lower than for the titrations done in July 2019 (see Figure 1). However, at k = 2, this is only significant for Sample F, and it is barely significant in that case. Again, a likely explanation for the systematic change is the low relative humidity in December. In such circumstances, a sample can lose moisture during the weighing process, which exposes the sample to air for a few minutes.

Table 2. The results of KF titrations on six adamantane samples.

Sample (injection#)	sample mass / g	H_2O / µg	$[H_2O]$ / µg g^{-1}	Average $[H_2O]$ / µg g^{-1}	Std Dev / µg g^{-1}	u_{blank} / µg g^{-1}	u_{offset} / µg g^{-1}	u_c / µg g^{-1}
A (5)	0.1204	59.6	419.3					
A (6)	0.1115	53.2	395.4					
A (7)	0.1119	46.7	335.9	**383.5**	35.1	19.8	5.9	**40.7**
B (5)	0.1874	97.8	473.2					
B (6)	0.1864	93.0	150.0					
B (7)	0.1873	88.6	424.4					
B (8)	0.1122	58.8	442.8	**447.6**	17.5	14.2	6.9	**23.5**
C (1)	0.1103	44.3	319.0					
C (2)	0.1258	70.8	490.3					
C (3)	0.1295	72.7	491.0	**433.4**	80.9	18.7	6.7	**83.3**
D (1)	0.1098	60.1	464.3					
D (2)	0.1140	60.4	449.9					
D (3)	0.1150	60.3	445.1	**453.1**	8.2	20.1	7.0	**22.8**
E (1)	0.1069	51.4	395.5					
E (2)	0.1068	51.0	392.2					
E (3)	0.1124	51.2	374.4	**387.4**	9.3	20.9	6.0	**23.6**
F (1)	0.1181	59.2	424.1					
F (2)	0.1135	56.1	414.0					
F (3)	0.1063	45.9	346.0	**394.7**	34.7	20.2	6.1	**40.6**

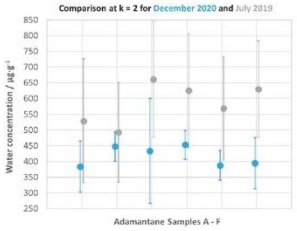

Figure 1. Comparison of adamantane sample A – F from July 2019 with the new titrations. The error bars represent the combined expanded uncertainties (k = 2) of the measurements.

FINAL NOTE: I attempted to analyze these adamantane samples using the new KF oven accessory, which is designed for use with solid samples (or low solubility or reactive samples). However, the high vapor pressure of adamantane at 150 °C caused significant sublimation of the sample into the top of the sample vial and into the (cooler) transfer line from the oven to the titrator. Unfortunately, significant flow rate changes, due to the resulting obstruction of the transfer line, spoiled the measurements with the KF oven.

[1] *Certain commercial equipment, instruments, or materials are identified in this paper to foster understanding. Such identification does not imply recommendation or endorsement by NIST, nor does it imply that the materials or equipment identified are necessarily the best available for the purpose.*

Figure A.1.2. Results of water content analysis using Karl Fischer titration.

The adamantane RM material was also analyzed for water content via Karl Fischer (KF) titration. Results indicate no statistical difference between the water content of the six measured samples (see Fig. A.1.2). Included in the KF analysis certificate are results for six additional adamantane samples, also labeled A – F, that were measured as part of exploratory work completed in 2019. It should be noted that the 2019 samples were from a different lot than the RM material and these results can therefore be ignored in the context of this work.

A.2. Baseline Determination

In this work, all measured heat flow curves were analyzed using TA Instruments' Universal Analysis software [29]. As was discussed in Secs. 3.1 and 3.2, the use of a simple linear baseline was not appropriate because the different heat capacities of the two crystalline phases of adamantane result in a significant offset between the baselines on either side of the transition peak. For instances such as these, the software includes a sigmoidal baseline option. This is an s-shaped line that is adjusted for the "fraction reacted" (α) versus time [29]. According to the software manual, the baseline is initially calculated as a straight line between the designated peak start and end points; it is then recalculated as the weighted average between the two projected baselines at the peak start and end (i.e., the initial and final baselines) [29]. The projected baselines can be constructed as either horizontal ("sigmoidal horizontal") or tangent ("sigmoidal tangent") baselines. In this work, the sigmoidal tangent baseline was used to account for any curvature in the baselines on either side of the transition. Mathematically, the sigmoidal baseline can be expressed as

$$\phi_{base} = (1 - \alpha)\phi_{init} + \alpha\phi_{final} \tag{A1}$$

where ϕ represents the heat flow rate for the sigmoidal baseline ("base"), the extrapolated initial baseline ("init"), and the extrapolated final baseline ("final"), respectively [11, 30]. With the sigmoidal tangent baseline, the initial and final baselines are constructed as tangent lines fit within specified endpoint pairs on either side of the peak. In Eq. (A1), $(1 - \alpha)$ and α represent the weighting factors for the aforementioned weighted average. Determination of the sigmoidal baseline is an iterative process where the area is calculated for each new baseline and compared to the previous area; the sigmoidal curve is repeatedly shifted until two consecutive area calculations differ by less than 1% [29]. Additional details regarding sigmoidal baseline construction can be found in van der Plaats [30] and Höhne et al. [11].

A.3. Transition Temperature Measurement Results

Individual replicate transition temperature measurement results (t_{meas}) for all samples are shown in Table A.3.1. Also included in the table are the corresponding sample mass, the measured heating rate (β_{avg}), and the combined standard uncertainty in transition temperature ($u(t_{meas})$). Results have been sorted by heating rate and sample mass; at each

heating rate, for a given sample, results are reported in the order the measurements were made.

Table A.3.1. Replicate Transition Temperature Measurements for Fifteen RM 8103 Samples at Four Heating Rates.

Sample	Mass (mg)	$\beta_{avg}{}^{a}$ (°C·min^{-1})	$t_{meas}{}^{b}$ (°C)	$u(t_{meas})^{c}$ (°C)
B	7.314	1.001	-64.47	0.12
B	7.314	1.000	-64.47	0.12
B	7.314	1.000	-64.46	0.12
A3	8.374	1.000	-64.47	0.12
A3	8.374	1.000	-64.48	0.12
A3	8.374	1.000	-64.48	0.12
A1	8.380	1.000	-64.45	0.12
A1	8.380	1.000	-64.46	0.12
A1	8.380	1.000	-64.45	0.12
C1	8.388	1.000	-64.48	0.12
C1	8.388	1.000	-64.46	0.12
C1	8.388	1.000	-64.45	0.12
C3	8.402	1.000	-64.49	0.12
C3	8.402	1.000	-64.49	0.12
C3	8.402	1.000	-64.49	0.12
A2	8.402	1.000	-64.46	0.12
A2	8.402	1.000	-64.47	0.12
A2	8.402	1.000	-64.45	0.12
B2	8.415	1.000	-64.53	0.12
B2	8.415	1.000	-64.54	0.12
B2	8.415	1.000	-64.54	0.12
A4	8.424	1.000	-64.55	0.12
A4	8.424	1.000	-64.56	0.12
A4	8.424	1.000	-64.54	0.12
C2	8.434	1.000	-64.51	0.12
C2	8.434	1.000	-64.49	0.12
C2	8.434	1.000	-64.51	0.12
F2	9.171	1.000	-64.43	0.12
F2	9.171	1.000	-64.44	0.12

Table A.3.1. continued

Sample	Mass (mg)	$\beta_{avg}{}^{a}$ (°C·min^{-1})	$t_{meas}{}^{b}$ (°C)	$u(t_{meas})^{c}$ (°C)
F2	9.171	1.000	-64.43	0.12
E2	9.227	1.000	-64.53	0.12
E2	9.227	1.000	-64.54	0.12
E2	9.227	1.000	-64.54	0.12
E	9.377	1.000	-64.46	0.12
E	9.377	1.000	-64.47	0.12
E	9.377	1.000	-64.48	0.12
F1	10.825	1.000	-64.44	0.12
F1	10.825	1.000	-64.46	0.12
F1	10.825	1.000	-64.48	0.12
D	14.459	1.000	-64.47	0.12
D	14.459	1.000	-64.48	0.12
D	14.459	1.000	-64.48	0.12
D2	14.502	1.000	-64.55	0.12
D2	14.502	1.000	-64.55	0.12
D2	14.502	1.000	-64.56	0.12
B	7.314	2.999	-64.45	0.12
B	7.314	2.999	-64.45	0.12
B	7.314	2.999	-64.48	0.12
A3	8.374	2.998	-64.47	0.12
A3	8.374	2.998	-64.49	0.12
A3	8.374	2.998	-64.47	0.12
A1	8.380	2.999	-64.45	0.12
A1	8.380	2.999	-64.45	0.12
A1	8.380	2.999	-64.49	0.12
C1	8.388	2.999	-64.47	0.12
C1	8.388	2.999	-64.42	0.12
C1	8.388	2.999	-64.48	0.12
C3	8.402	2.998	-64.49	0.12
C3	8.402	2.999	-64.48	0.12
C3	8.402	2.999	-64.50	0.12
A2	8.402	2.999	-64.49	0.12
A2	8.402	2.999	-64.41	0.12

Table A.3.1. continued

Sample	Mass (mg)	$\beta_{avg}{}^{a}$ (°C·min^{-1})	$t_{meas}{}^{b}$ (°C)	$u(t_{meas})^{c}$ (°C)
A2	8.402	2.999	-64.48	0.12
B2	8.415	2.999	-64.56	0.12
B2	8.415	2.998	-64.57	0.12
B2	8.415	2.998	-64.56	0.12
A4	8.424	2.998	-64.55	0.12
A4	8.424	2.999	-64.56	0.12
A4	8.424	2.998	-64.57	0.12
C2	8.434	2.999	-64.50	0.12
C2	8.434	2.998	-64.49	0.12
C2	8.434	2.999	-64.51	0.12
F2	9.171	2.998	-64.46	0.12
F2	9.171	2.999	-64.45	0.12
F2	9.171	2.999	-64.45	0.12
E2	9.227	2.998	-64.51	0.12
E2	9.227	2.999	-64.49	0.12
E2	9.227	2.999	-64.51	0.12
E	9.377	2.998	-64.47	0.12
E	9.377	2.999	-64.48	0.12
E	9.377	2.998	-64.45	0.12
F1	10.825	2.998	-64.48	0.12
F1	10.825	2.998	-64.49	0.12
F1	10.825	2.998	-64.47	0.12
D	14.459	2.998	-64.46	0.12
D	14.459	2.998	-64.51	0.12
D	14.459	2.998	-64.52	0.12
D2	14.502	2.998	-64.56	0.12
D2	14.502	2.998	-64.57	0.12
D2	14.502	2.998	-64.57	0.12
B	7.314	4.996	-64.45	0.17
B	7.314	4.996	-64.44	0.17
B	7.314	4.996	-64.47	0.17
A3	8.374	4.996	-64.50	0.17
A3	8.374	4.996	-64.49	0.17

Table A.3.1. continued

Sample	Mass (mg)	$\beta_{avg}{}^{a}$ (°C·min^{-1})	$t_{meas}{}^{b}$ (°C)	$u(t_{meas})^{c}$ (°C)
A3	8.374	4.995	-64.52	0.17
A1	8.380	4.996	-64.49	0.17
A1	8.380	4.996	-64.46	0.17
A1	8.380	4.995	-64.46	0.17
C1	8.388	4.996	-64.47	0.17
C1	8.388	4.995	-64.49	0.17
C1	8.388	4.996	-64.47	0.17
C3	8.402	4.996	-64.51	0.17
C3	8.402	4.996	-64.49	0.17
C3	8.402	4.995	-64.51	0.17
A2	8.402	4.995	-64.48	0.17
A2	8.402	4.996	-64.48	0.17
A2	8.402	4.996	-64.51	0.17
B2	8.415	4.995	-64.57	0.17
B2	8.415	4.995	-64.60	0.17
B2	8.415	4.995	-64.59	0.17
A4	8.424	4.995	-64.56	0.17
A4	8.424	4.995	-64.57	0.17
A4	8.424	4.996	-64.56	0.17
C2	8.434	4.996	-64.53	0.17
C2	8.434	4.996	-64.53	0.17
C2	8.434	4.995	-64.53	0.17
F2	9.171	4.996	-64.45	0.17
F2	9.171	4.995	-64.48	0.17
F2	9.171	4.995	-64.46	0.17
E2	9.227	4.995	-64.56	0.17
E2	9.227	4.995	-64.52	0.17
E2	9.227	4.995	-64.56	0.17
E	9.377	4.995	-64.49	0.17
E	9.377	4.995	-64.49	0.17
E	9.377	4.995	-64.45	0.17
F1	10.825	4.995	-64.47	0.17
F1	10.825	4.995	-64.46	0.17
F1	10.825	4.995	-64.47	0.17

Table A.3.1. continued

Sample	Mass (mg)	$\beta_{avg}{}^{a}$ (°C·min^{-1})	$t_{meas}{}^{b}$ (°C)	$u(t_{meas})^{c}$ (°C)
D	14.459	4.993	-64.52	0.17
D	14.459	4.993	-64.53	0.17
D	14.459	4.993	-64.53	0.17
D2	14.502	4.993	-64.58	0.17
D2	14.502	4.994	-64.57	0.17
D2	14.502	4.993	-64.58	0.17
B	7.314	9.979	-64.40	0.31
B	7.314	9.980	-64.42	0.31
B	7.314	9.978	-64.43	0.31
A3	8.374	9.977	-64.49	0.31
A3	8.374	9.977	-64.42	0.31
A3	8.374	9.977	-64.43	0.31
A1	8.380	9.977	-64.49	0.31
A1	8.380	9.976	-64.44	0.31
A1	8.380	9.977	-64.41	0.31
C1	8.388	9.976	-64.48	0.31
C1	8.388	9.977	-64.49	0.31
C1	8.388	9.978	-64.45	0.31
C3	8.402	9.977	-64.44	0.31
C3	8.402	9.978	-64.47	0.31
C3	8.402	9.977	-64.18	0.31
A2	8.402	9.976	-64.42	0.31
A2	8.402	9.976	-64.41	0.31
A2	8.402	9.975	-64.44	0.31
B2	8.415	9.975	-64.32	0.31
B2	8.415	9.975	-64.57	0.31
B2	8.415	9.977	-64.33	0.31
A4	8.424	9.978	-64.54	0.31
A4	8.424	9.976	-64.51	0.31
A4	8.424	9.977	-64.51	0.31
C2	8.434	9.976	-64.53	0.31
C2	8.434	9.977	-64.50	0.31
C2	8.434	9.976	-64.49	0.31

Table A.3.1. continued

Sample	Mass (mg)	β_{avg} [a] (°C·min^{-1})	t_{meas} [b] (°C)	$u(t_{meas})$ [c] (°C)
F2	9.171	9.975	-64.42	0.31
F2	9.171	9.976	-64.45	0.31
F2	9.171	9.975	-64.46	0.31
E2	9.227	9.976	-64.54	0.31
E2	9.227	9.975	-64.55	0.31
E2	9.227	9.975	-64.35	0.31
E	9.377	9.976	-64.42	0.31
E	9.377	9.975	-64.45	0.31
E	9.377	9.976	-64.44	0.31
F1	10.825	9.974	-64.47	0.31
F1	10.825	9.973	-64.46	0.31
F1	10.825	9.973	-64.46	0.31
D	14.459	9.970	-64.51	0.31
D	14.459	9.968	-64.53	0.31
D	14.459	9.971	-64.51	0.31
D2	14.502	9.971	-64.59	0.31
D2	14.502	9.971	-64.58	0.31
D2	14.502	9.971	-64.59	0.31

[a]Measured heating rate. [b]Measured transition temperature. [c]Combined standard uncertainty.

A.4. Enthalpy of Transition Measurement Results

Individual replicate enthalpy of transition measurement results (ΔH_{meas}) for all samples are shown in Table A.4.1. Also included in the table are the corresponding sample mass, the measured heating rate (β_{avg}), and the combined standard uncertainty in enthalpy ($u(\Delta H_{meas})$). Results have been sorted by heating rate and sample mass; at each heating rate, for a given sample, results are reported in the order the measurements were made.

Table A.4.1. Replicate Enthalpy of Transition Measurements for Fifteen RM 8103 Samples at Four Heating Rates.

Sample	Mass (mg)	β_{avg} [a] (°C·min^{-1})	ΔH_{meas} [b] (J·g^{-1})	$u(\Delta H_{meas})$ [c] (J·g^{-1})
B	7.314	1.001	21.85	0.30
B	7.314	1.000	22.01	0.30
B	7.314	1.000	21.88	0.30

Table A.4.1. continued

Sample	Mass (mg)	β_{avg} [a] (°C·min^{-1})	ΔH_{meas} [b] (J·g^{-1})	$u(\Delta H_{meas})$ [c] (J·g^{-1})
A3	8.374	1.000	22.21	0.30
A3	8.374	1.000	22.16	0.30
A3	8.374	1.000	22.10	0.30
A1	8.380	1.000	22.05	0.30
A1	8.380	1.000	21.82	0.30
A1	8.380	1.000	22.13	0.30
C1	8.388	1.000	22.02	0.30
C1	8.388	1.000	21.89	0.30
C1	8.388	1.000	22.01	0.30
C3	8.402	1.000	22.03	0.30
C3	8.402	1.000	21.64	0.30
C3	8.402	1.000	22.24	0.30
A2	8.402	1.000	22.05	0.30
A2	8.402	1.000	22.10	0.30
A2	8.402	1.000	22.08	0.30
B2	8.415	1.000	21.96	0.30
B2	8.415	1.000	22.13	0.30
B2	8.415	1.000	22.10	0.30
A4	8.424	1.000	21.73	0.30
A4	8.424	1.000	21.87	0.30
A4	8.424	1.000	21.88	0.30
C2	8.434	1.000	21.78	0.30
C2	8.434	1.000	21.70	0.30
C2	8.434	1.000	21.77	0.30
F2	9.171	1.000	22.15	0.30
F2	9.171	1.000	22.06	0.30
F2	9.171	1.000	21.98	0.30
E2	9.227	1.000	21.81	0.30
E2	9.227	1.000	21.83	0.30
E2	9.227	1.000	21.91	0.30
E	9.377	1.000	21.85	0.30
E	9.377	1.000	22.07	0.30
E	9.377	1.000	21.68	0.30
F1	10.825	1.000	21.93	0.30

Table A.4.1. continued

Sample	Mass (mg)	$\beta_{avg}{}^{a}$ (°C·min^{-1})	$\Delta H_{meas}{}^{b}$ (J·g^{-1})	$u(\Delta H_{meas})^{c}$ (J·g^{-1})
F1	10.825	1.000	21.89	0.30
F1	10.825	1.000	21.75	0.30
D	14.459	1.000	21.83	0.30
D	14.459	1.000	21.88	0.30
D	14.459	1.000	21.70	0.30
D2	14.502	1.000	22.15	0.30
D2	14.502	1.000	22.15	0.30
D2	14.502	1.000	21.99	0.30
B	7.314	2.999	21.49	0.15
B	7.314	2.999	21.73	0.15
B	7.314	2.999	21.78	0.15
A3	8.374	2.998	21.81	0.15
A3	8.374	2.998	21.90	0.15
A3	8.374	2.998	21.87	0.15
A1	8.380	2.999	21.67	0.15
A1	8.380	2.999	21.83	0.15
A1	8.380	2.999	21.83	0.15
C1	8.388	2.999	21.79	0.15
C1	8.388	2.999	21.11	0.15
C1	8.388	2.999	21.85	0.15
C3	8.402	2.998	21.88	0.15
C3	8.402	2.999	21.81	0.15
C3	8.402	2.999	21.87	0.15
A2	8.402	2.999	21.89	0.15
A2	8.402	2.999	21.04	0.15
A2	8.402	2.999	21.87	0.15
B2	8.415	2.999	21.85	0.15
B2	8.415	2.998	21.94	0.15
B2	8.415	2.998	21.96	0.15
A4	8.424	2.998	21.81	0.15
A4	8.424	2.999	21.91	0.15
A4	8.424	2.998	21.86	0.15
C2	8.434	2.999	21.77	0.15

Table A.4.1. continued

Sample	Mass (mg)	$\beta_{avg}{}^{a}$ (°C·min^{-1})	$\Delta H_{meas}{}^{b}$ (J·g^{-1})	$u(\Delta H_{meas})^{c}$ (J·g^{-1})
C2	8.434	2.998	21.84	0.15
C2	8.434	2.999	21.84	0.15
F2	9.171	2.998	21.84	0.15
F2	9.171	2.999	21.70	0.15
F2	9.171	2.999	21.84	0.15
E2	9.227	2.998	21.35	0.15
E2	9.227	2.999	21.03	0.15
E2	9.227	2.999	21.28	0.15
E	9.377	2.998	21.75	0.15
E	9.377	2.999	21.78	0.15
E	9.377	2.998	21.89	0.15
F1	10.825	2.998	21.80	0.15
F1	10.825	2.998	21.75	0.15
F1	10.825	2.998	21.79	0.15
D	14.459	2.998	21.11	0.15
D	14.459	2.998	21.85	0.15
D	14.459	2.998	21.88	0.15
D2	14.502	2.998	21.91	0.15
D2	14.502	2.998	21.99	0.15
D2	14.502	2.998	22.01	0.15
B	7.314	4.996	21.79	0.10
B	7.314	4.996	21.79	0.10
B	7.314	4.996	21.86	0.10
A3	8.374	4.996	22.04	0.10
A3	8.374	4.996	21.97	0.10
A3	8.374	4.995	22.06	0.10
A1	8.380	4.996	21.78	0.10
A1	8.380	4.996	21.93	0.10
A1	8.380	4.995	21.83	0.10
C1	8.388	4.996	21.90	0.10
C1	8.388	4.995	21.85	0.10
C1	8.388	4.996	21.95	0.10
C3	8.402	4.996	21.96	0.10

Table A.4.1. continued

Sample	Mass (mg)	β_{avg} [a] (°C·min^{-1})	ΔH_{meas} [b] (J·g^{-1})	$u(\Delta H_{meas})$ [c] (J·g^{-1})
C3	8.402	4.996	21.34	0.10
C3	8.402	4.995	21.98	0.10
A2	8.402	4.995	21.95	0.10
A2	8.402	4.996	21.91	0.10
A2	8.402	4.996	21.93	0.10
B2	8.415	4.995	21.92	0.10
B2	8.415	4.995	21.99	0.10
B2	8.415	4.995	21.95	0.10
A4	8.424	4.995	21.91	0.10
A4	8.424	4.995	21.97	0.10
A4	8.424	4.996	21.95	0.10
C2	8.434	4.996	21.88	0.10
C2	8.434	4.996	21.89	0.10
C2	8.434	4.995	21.86	0.10
F2	9.171	4.996	21.92	0.10
F2	9.171	4.995	21.98	0.10
F2	9.171	4.995	21.95	0.10
E2	9.227	4.995	21.91	0.10
E2	9.227	4.995	21.31	0.10
E2	9.227	4.995	21.42	0.10
E	9.377	4.995	21.87	0.10
E	9.377	4.995	21.81	0.10
E	9.377	4.995	21.21	0.10
F1	10.825	4.995	21.77	0.10
F1	10.825	4.995	21.79	0.10
F1	10.825	4.995	21.47	0.10
D	14.459	4.993	21.92	0.10
D	14.459	4.993	21.91	0.10
D	14.459	4.993	21.91	0.10
D2	14.502	4.993	22.07	0.10
D2	14.502	4.994	21.97	0.10
D2	14.502	4.993	21.99	0.10
B	7.314	9.979	22.19	0.32

Table A.4.1. continued

Sample	Mass (mg)	β_{avg} [a] (°C·min^{-1})	ΔH_{meas} [b] (J·g^{-1})	$u(\Delta H_{meas})$ [c] (J·g^{-1})
B	7.314	9.980	22.19	0.32
B	7.314	9.978	22.18	0.32
A3	8.374	9.977	22.43	0.32
A3	8.374	9.977	22.27	0.32
A3	8.374	9.977	22.37	0.32
A1	8.380	9.977	22.46	0.32
A1	8.380	9.976	22.36	0.32
A1	8.380	9.977	22.23	0.32
C1	8.388	9.976	22.50	0.32
C1	8.388	9.977	22.43	0.32
C1	8.388	9.978	22.20	0.32
C3	8.402	9.977	22.37	0.32
C3	8.402	9.978	22.42	0.32
C3	8.402	9.977	21.01	0.32
A2	8.402	9.976	22.37	0.32
A2	8.402	9.976	22.24	0.32
A2	8.402	9.975	22.38	0.32
B2	8.415	9.975	21.17	0.32
B2	8.415	9.975	22.43	0.32
B2	8.415	9.977	21.09	0.32
A4	8.424	9.978	22.40	0.32
A4	8.424	9.976	22.25	0.32
A4	8.424	9.977	22.22	0.32
C2	8.434	9.976	22.34	0.32
C2	8.434	9.977	22.27	0.32
C2	8.434	9.976	22.18	0.32
F2	9.171	9.975	22.39	0.32
F2	9.171	9.976	22.45	0.32
F2	9.171	9.975	22.45	0.32
E2	9.227	9.976	22.39	0.32
E2	9.227	9.975	22.32	0.32
E2	9.227	9.975	21.35	0.32
E	9.377	9.976	22.23	0.32
E	9.377	9.975	22.31	0.32

Table A.4.1. continued

Sample	Mass (mg)	β_{avg} [a] (°C·min^{-1})	ΔH_{meas} [b] (J·g^{-1})	$u(\Delta H_{meas})$ [c] (J·g^{-1})
E	9.377	9.976	22.30	0.32
F1	10.825	9.974	22.33	0.32
F1	10.825	9.973	22.26	0.32
F1	10.825	9.973	22.34	0.32
D	14.459	9.970	22.31	0.32
D	14.459	9.968	22.43	0.32
D	14.459	9.971	22.44	0.32
D2	14.502	9.971	22.49	0.32
D2	14.502	9.971	22.46	0.32
D2	14.502	9.971	22.56	0.32

[a]Measured heating rate. [b]Measured enthalpy of transition. [c]Combined standard uncertainty.

A.5. Hierarchical Bayesian Model Posterior Predictive Checks

We performed posterior predictive checks to verify that the hierarchical Bayes model and its results discussed in Secs. 3.1 and 3.2 are reasonable. Specifically, we use the model and samples from the posterior to predict new values of t_{meas} and ΔH_{meas}. In Fig. A.5.1, we compare histograms of the observed values to the predicted values for t_{meas}, while in Fig. A.5.2 we compare the results for ΔH_{meas}. In both figures, the row marked "Observed" shows the measured data; for example, the histogram on the first row under β = 1 °C·min^{-1} summarizes all measured values at that nominal heating rate.

Additionally, each histogram for the "Simulated" data summarizes a randomly generated set of 45 predicted values, matching the size of the observed samples. These predicted values are simulated by plugging posterior samples of the parameter values into the model we defined in Eq. (1) for t_{meas} and Eq. (3) for ΔH_{meas}. We generated five sets of these for each β value. These predicted values are depicted in rows below the corresponding true histogram; for example, rows 2 – 6 of the first column show five separate sets of samples simulated from the posterior distribution for β = 1 °C·min^{-1}. In all cases, the histograms of samples from the predicted values look reasonably similar to the observed data, indicating that the proposed model is reasonable for this data.

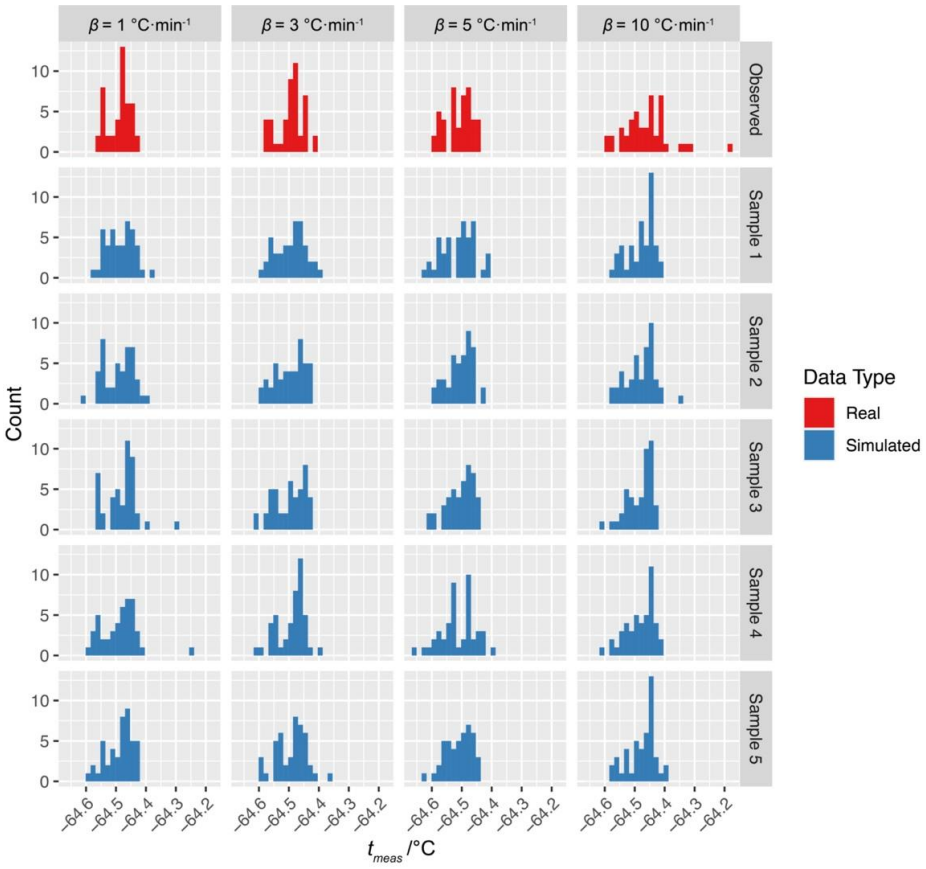

Figure A.5.1. Histogram results of posterior predictive checks for t_{meas}. Measured transition temperatures are shown in red for each of the four nominal heating rates. Simulated predicted transition temperatures are shown in blue. Five separate sets of simulated samples are shown for each of the four nominal heating rates.

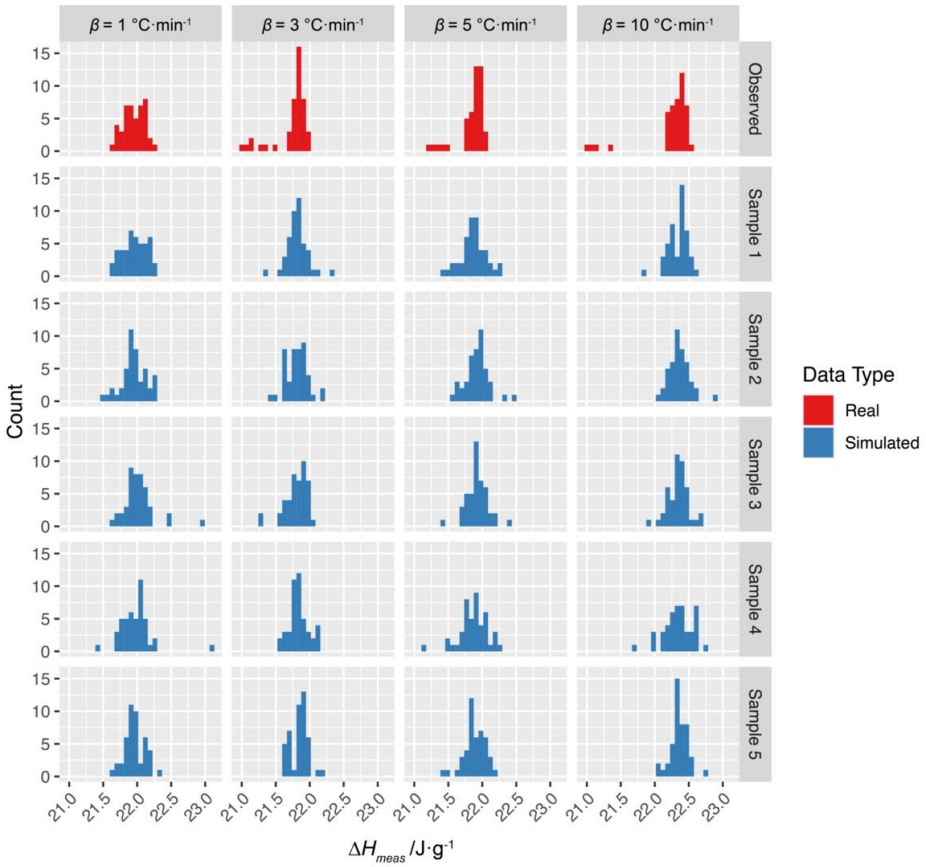

Figure A.5.2. Histogram results of posterior predictive checks for ΔH_{meas}. Measured enthalpies of transition are shown in red for each of the four nominal heating rates. Simulated predicted enthalpies of transition are shown in blue. Five separate sets of simulated samples are shown for each of the four nominal heating rates.